applied sciences

MDPI

Review

Non-Surgical Treatment for Hepatocellular Carcinoma: What to Expect at Follow-Up Magnetic Resonance Imaging—A Pictorial Review

Andreea-Elena Scheau [1], Sandra Oana Jurca [1], Cristian Scheau [2,3,*] and Ioana Gabriela Lupescu [1,4]

[1] Department of Radiology and Medical Imaging, Fundeni Clinical Institute, 022328 Bucharest, Romania
[2] Department of Physiology, The "Carol Davila" University of Medicine and Pharmacy, 050474 Bucharest, Romania
[3] Department of Radiology and Medical Imaging, "Foisor" Clinical Hospital of Orthopaedics, Traumatology and Osteoarticular TB, 030167 Bucharest, Romania
[4] Department of Radiology, Medical Imaging and Interventional Radiology, The "Carol Davila" University of Medicine and Pharmacy, 050474 Bucharest, Romania
* Correspondence: cristian.scheau@umfcd.ro

Abstract: Hepatocellular carcinoma (HCC), the most prevalent form of liver cancer, represents a significant global health challenge due to its rising incidence, complex management, as well as recurrence rates of up to 70% or more. Early and accurate imaging diagnosis, through modalities such as ultrasound, CT, and MRI, is crucial for effective treatment. Minimally invasive therapies, including thermal ablation methods such as radiofrequency ablation, microwave ablation, laser ablation, high-intensity focused ultrasound, and cryoablation, as well as non-thermal methods like percutaneous ethanol injection and irreversible electroporation, have shown promise in treating early and intermediate stages of HCC. Some studies have reported complete response in more than 90% of nodules and survival rates of up to 60–85% at 5 years after the procedure. These therapies are increasingly employed and induce specific morphological and physiological changes in the tumor and surrounding liver tissue, which are critical to monitor for assessing treatment efficacy and detecting recurrence. This review highlights the imaging characteristics of HCC following non-surgical treatments, focusing on the common features, challenges in post-treatment evaluation, and the importance of standardized imaging protocols such as the Liver Imaging Reporting and Data System. Understanding these imaging features is essential for radiologists to accurately assess tumor viability and guide further therapeutic decisions, ultimately improving patient outcomes.

Keywords: hepatocellular carcinoma; magnetic resonance imaging; diagnosis; follow-up; minimally invasive treatment; morphological features; tumor recurrence; tumor viability

Citation: Scheau, A.-E.; Jurca, S.O.; Scheau, C.; Lupescu, I.G. Non-Surgical Treatment for Hepatocellular Carcinoma: What to Expect at Follow-Up Magnetic Resonance Imaging—A Pictorial Review. *Appl. Sci.* **2024**, *14*, 9159. https://doi.org/10.3390/app14209159

Academic Editors: Dermatas Evangelos, Athanasios Koutras, Ioanna Christoyianni and George Apostolopoulos

Received: 4 September 2024
Revised: 3 October 2024
Accepted: 7 October 2024
Published: 10 October 2024

1. Introduction

Hepatocellular carcinoma (HCC) is the most common type of liver cancer and a significant contributor to the global cancer burden [1]. With incidence rates rising in many countries and an estimated overall incidence higher than one million cases within the next three years, HCC is a major challenge for healthcare systems worldwide and an important research focus [2].

Patients with liver cirrhosis are screened for HCC with ultrasound and any suspicion of malignancy is clarified based on specific imaging features seen on Computed Tomography (CT) or Magnetic Resonance Imaging (MRI) [3]. Due to the high specificity of imaging findings, the initial diagnosis can be set solely on imaging features without requiring liver biopsy in the majority of cases [4]. However, rare manifestations of HCC and confounding aspects of recurrence of treated HCC may prove to be diagnostic challenges, and the high recurrence rates of up to 70% at 5 years after treatment increase the complexity of the case management [5–8]. Currently, practice guidelines from various scientific and professional

groups are available to assist the radiologist in improving the diagnosis rate and staging accuracy and are updated every few years, with new recommendations made available in 2024 [9–11].

The Liver Imaging Reporting and Data System (LI-RADS) is designed to standardize image reporting of HCC nodules, and the 2018 version includes a section on reporting treated HCC, named LI-RADS treatment response (LR-TR) [12]. This includes definitions and precise instructions for size and enhancement measurements of the nodules and the tumor viable tissue, if present. However, the minimally invasive treatment can induce local morphological changes specific to the method, that may represent a challenge for the radiologist in correctly assessing tumor tissue viability.

In terms of HCC management, the Barcelona Clinic Liver Cancer (BCLC) prognosis and treatment strategy is one of the most commonly referred to guides for clinical practice and therapeutic decision-making [13]. As per the 2022 BCLC strategy, minimally invasive treatment is recommended for intermediate-stage patients as well as some early-stage cases. There are multiple therapeutic options classified as minimally invasive, each with specific indications and recommendations [14]. Patients undergoing these treatments will be routinely monitored for tumor viability and recurrence, and since local therapies can induce morphological changes to the adjacent tissues, correctly identifying viability may prove challenging [15].

The purpose of this review is to highlight the most common imaging features of HCC nodules after minimally invasive procedures and to draw attention to critical aspects that may require additional diagnostics steps or close surveillance.

2. Minimally Invasive Therapies for HCC and Their Tissular Effects

A large variety of therapeutic choices are available for HCC patients and selection of the optimal course is usually conducted according to BCLC criteria and patient liver function and concurring health issues [16]. Thermal and non-thermal ablation may be used with curative intent for patients in the very early and early stages of HCC, while patients with intermediate disease may benefit from transcatheter arterial chemoembolization (TACE) [16,17]. Surgical resection, liver transplantation, and molecular therapies, among others, are options for early, intermediate, and advanced stages of the disease [18,19], but do not fall within the scope of this paper.

Regarding the minimally invasive therapies, they rely on local tumor destruction through various mechanisms. In most cases, the result of a successful procedure is obtaining an area of coagulation necrosis that includes the tumor nodule and even goes beyond it by an intended and calculated safety margin [20]. Some procedures, such as TACE, can also induce liquefactive necrosis areas within the coagulation necrosis; this occurs due to the infiltration of neutrophils, which dissolve the necrotic material but fail to completely clear it from the area and this may contribute to hindering the venous or lymphatic drainage from the treated zone [21].

As mentioned before, minimally invasive treatments cause significant changes to the tumor and surrounding areas and may produce morphological and physiopathological changes with corresponding imaging features. The remainder of this section addresses the mechanism of action and expected effects on the tumor and adjacent liver tissue.

2.1. Thermal Ablative Therapies

Thermal ablative therapies use extreme temperatures to obtain tumor destruction. A schematic representation of their mechanisms of action is presented in Figure 1.

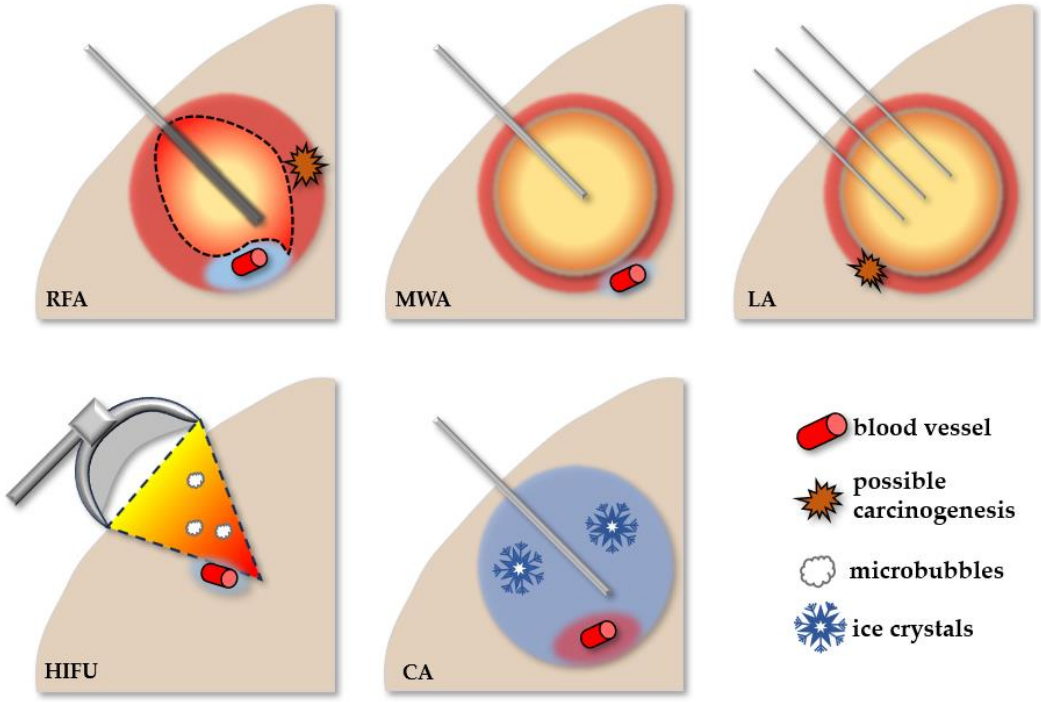

Figure 1. Overview of the thermal ablative therapies and their effects. RFA = radiofrequency ablation, MWA = microwave ablation, LA = laser ablation, HIFU = high-intensity focused ultrasound; CA = cryoablation.

2.1.1. Radiofrequency Ablation

Radiofrequency ablation (RFA) is commonly reserved for patients with HCC nodules smaller than 5 cm and several randomized trials have shown it to yield a 94% or higher complete response rate as well as a 54% or higher 5-year survival [22–26]. RFA essentially relies on tumor destruction through extreme heat obtained through high-frequency radiowaves between 460 and 480 kHz, but the range may be extended in some cases to 375–500 kHz or beyond [27]. The alternating electrical current travels through the path of least resistance and produces frictional heat ("electrical sink" effect) through ion agitation, which is focused inside the tumor nodule, inducing cellular damage [28]. When temperatures in the tissue reach 60 °C, instant coagulation of proteins and destruction of cellular components is obtained; however, exceeding 100 °C causes fluids to boil with vaporization that implies gas release in the area of ablation; this insulates the tissue and hampers the procedure [28,29]. Moreover, blood vessels can carry away the electrical current from the vicinity of the electrode, thereby decreasing the overall temperature in the region ("heat sink" effect), diminishing the effectiveness of the procedure and allowing for the possibility for some tumor cells to survive [22].

After several seconds of application, RFA induces an ellipsoid volume of coagulation necrosis in the targeted area around the electrode. Animal studies have shown that the histopathological changes induced by RFA are heterogeneous, with a central area of carbonization along the trajectory of the electrode surrounded by an area of necrosis and a peripheric hemorrhagic rim [30]. Moreover, the hemorrhagic rim appears to be surrounded by a fibrovascular halo that thickens over time [31]. There are reports that suggest that cell proliferation is stimulated within the hemorrhagic area and this mechanism could be responsible for the appearance of tumor recurrence [32]. Liver capsule retraction may be observed in the ablation of superficial tumors [33] (Figure 2).

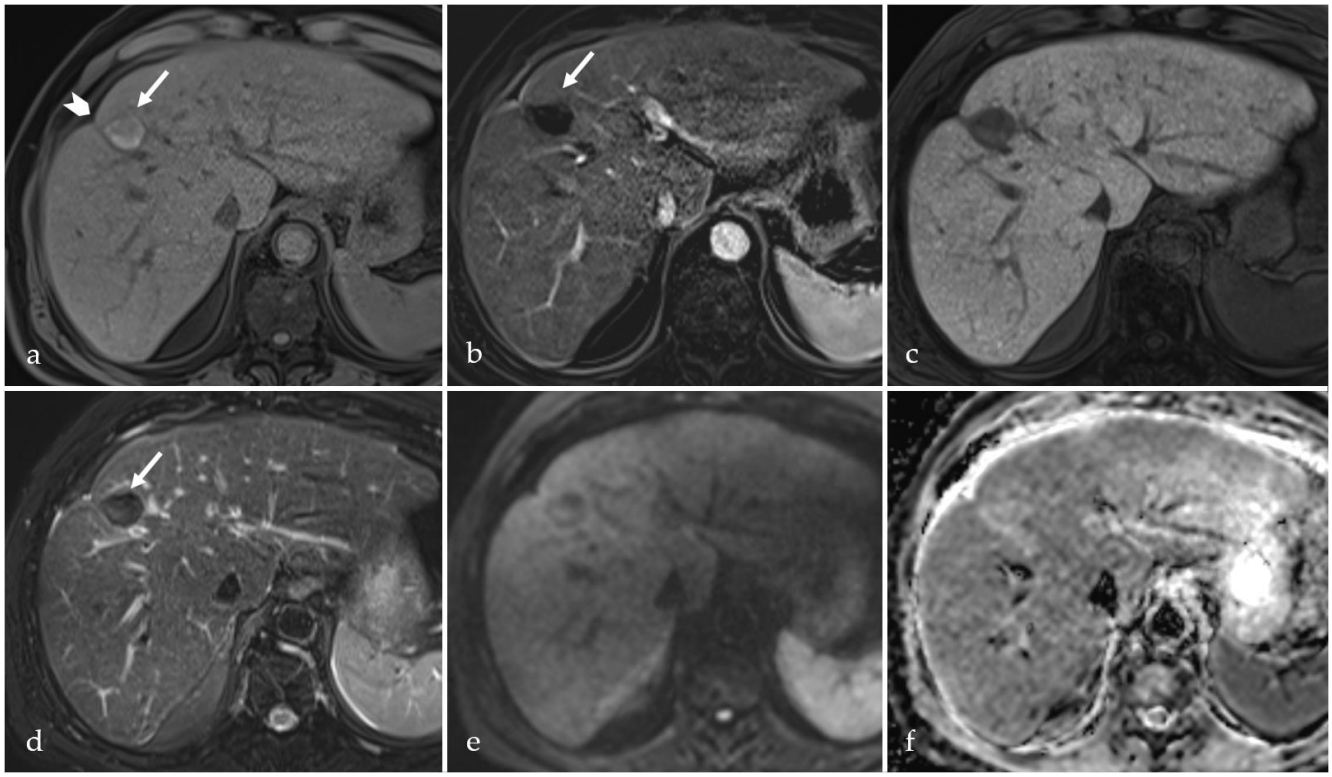

Figure 2. MRI examination with hepatospecific intravenous contrast of a patient with HCC in liver segment VIII, 5 months after RFA. Axial plane images: (**a**)—T1 weighted image with fat suppresion; (**b**)—subtraction image (obtained by subtracting a T1 fat saturated image without contrast enhancement from a T1 fat saturated image with contrast enhancement in the arterial phase; (**c**)—T1 WI with fat saturation in the hepatobiliary phase (obtained 20 min after contrast injection); (**d**)—T2 weighted image with fat saturation; (**e**)—diffusion weighted image; (**f**)—apparent diffusion coefficent map). There is an area of coagulative necrosis hyperintense on T1 fat-saturated images (arrow, (**a**,**b**)), hypointense on T2 fat sat (**d**), without restricted diffusion on DWI/ADC (**e**,**f**), non-enhancing in the arterial phase ((**b**), subtraction) or hepatobiliary phase (**c**). To better depict contrast enhancement in high-intensity T1 fat-saturated lesions, subtraction is a necessary tool. Also, there is capsular retraction on the needle path (chevron in (**a**)).

In order to perform a successful procedure and ensure all viable tumor cells are destroyed, a tumor-free margin of at least 1 cm thickness should be obtained around the tumor nodule [28].

2.1.2. Microwave Ablation

Microwave ablation (MWA) was applied in HCC patients with tumors smaller than 5 cm, obtaining complete nodule ablation in around 90% of cases with a 3-year recurrence-free period in around 30% of cases [34–36]; the method was also applied in patients with tumors larger than 5 cm, with good response rates [36,37]. MWA uses electromagnetic energy transmitting microwaves into the tissues at frequencies in the range of 300 MHz to 10 GHz, commonly at 915 MHz and 2.45 GHz [22,23]. No current is transmitted through the patient as the energy is focused through dedicated antennas. The passing of the microwaves causes friction of water and nearby molecules, generating heat in the process. Particular to this method is that the heat is instantaneous and homogeneous and is produced in the entire area where microwaves are conveyed ("near field") [23,38]. Therefore, local factors are less likely to influence the area and effectiveness of the MWA.

Studies on animal models and human liver explants have shown that MWA induces histologic changes consisting of three concentric areas: central necrosis surrounded by a thin brown capsule of cells with damaged membranes and a peripheric hemorrhagic

rim [39,40]. Within the central area of necrosis, gas bubbles and cavitation may be observed due to vaporization [41]. As also observed in RFA, blood clots and endothelial injuries may be seen in small and large vessels in the ablated area [40,42]. In the following hours, the ablation area appears to expand and reaches a maximum diameter at 12 h after the procedure, a consequence of the cellular and DNA damage in the margins of the treated zone [40,43]. A fibrous capsule develops around one week after MWA and resorption in the necrosis area causes the lesion to significantly decrease in size after several weeks [43] (Figure 3).

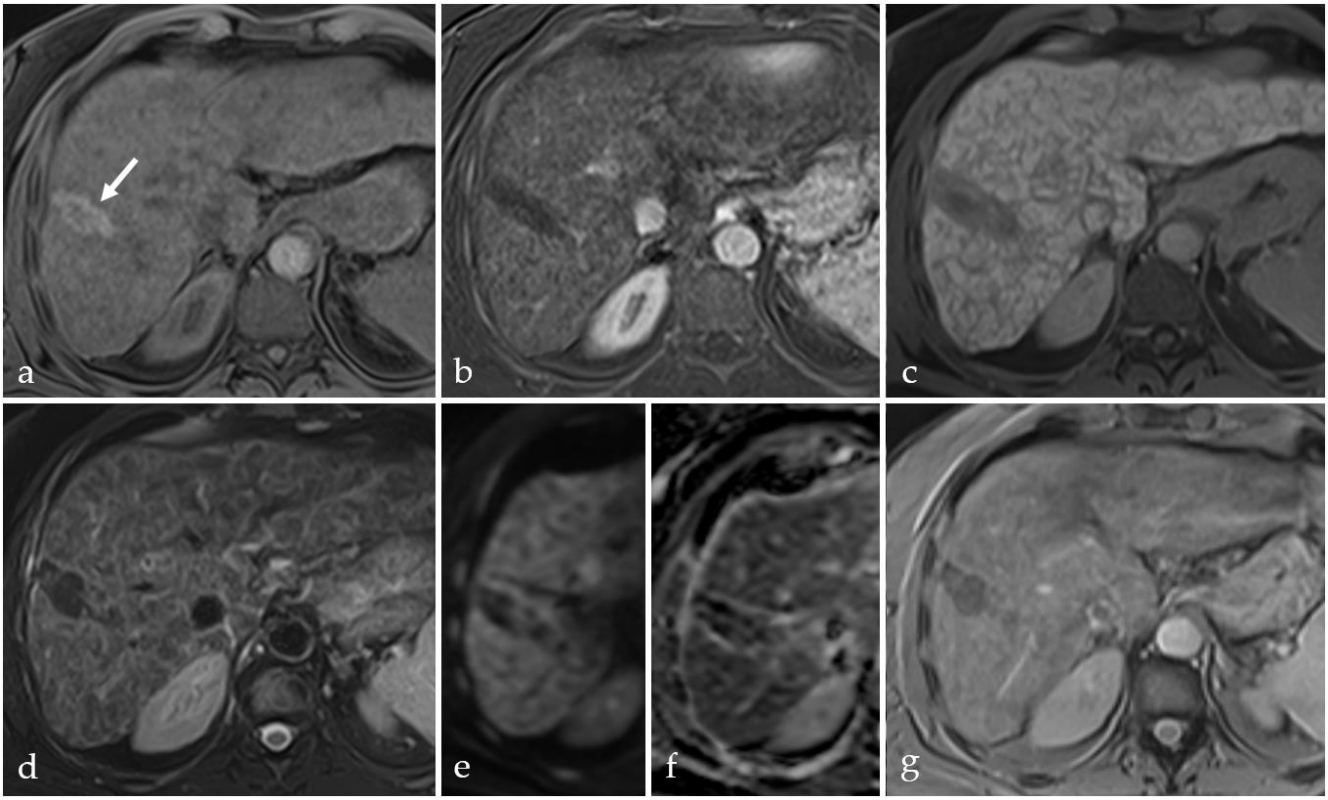

Figure 3. MRI examination of an HCC nodule in the right liver lobe, treated with MWA 2 months prior. (**a**) T1 weighted image with fat suppression; (**b**)—subtraction image; (**c**)—T1 WI with fat suppression in the hepatobiliary phase (at 20 min); (**d**)—T2 weighted image with fat saturation; (**e**)—diffusion weighted image; (**f**)—apparent diffusion coefficient map. Arrow in figure a points to an ellipsoid area of ablation, with MRI features of coagulative necrosis, but low signal intensity is observed on the T2* sequence (**g**), suggestive of chronic hemorrhage.

Technological advances in the devices and antennas allowed for improved success rates in treating HCC nodules; however, since vessels with diameters up to 6–7 mm are coagulated, vessel proximity remains a challenge in applying this therapeutic method [40,44].

2.1.3. Laser Ablation

Laser ablation (LA) requires the percutaneous insertion of an array of needles into the tumor that allows the passing of optic fibers that will emit near-infrared light. The method may be used for single or multinodular HCC with sizes usually up to 5 cm and yields a response rate of up to 97% and reported overall survival rates at 3 years of up to 68% [45–47]. LA commonly uses an Nd-YAG (neodymium: yttrium-aluminum-garnet) laser with either a shorter wavelength of 800–980 nm or a higher-tissue penetrating 1064 nm wavelength [48]. The released infrared energy induces heat in the area around the insertion. Similarly to RFA and MWA, cell death is obtained at temperatures above 60 °C, but exceeding 100 °C induces vaporization, which hinders the effectiveness of the method. Tissue carbonization,

which appears at over 300 °C, has even more significant effects in terms of limiting heat conduction [48] (Figure 4).

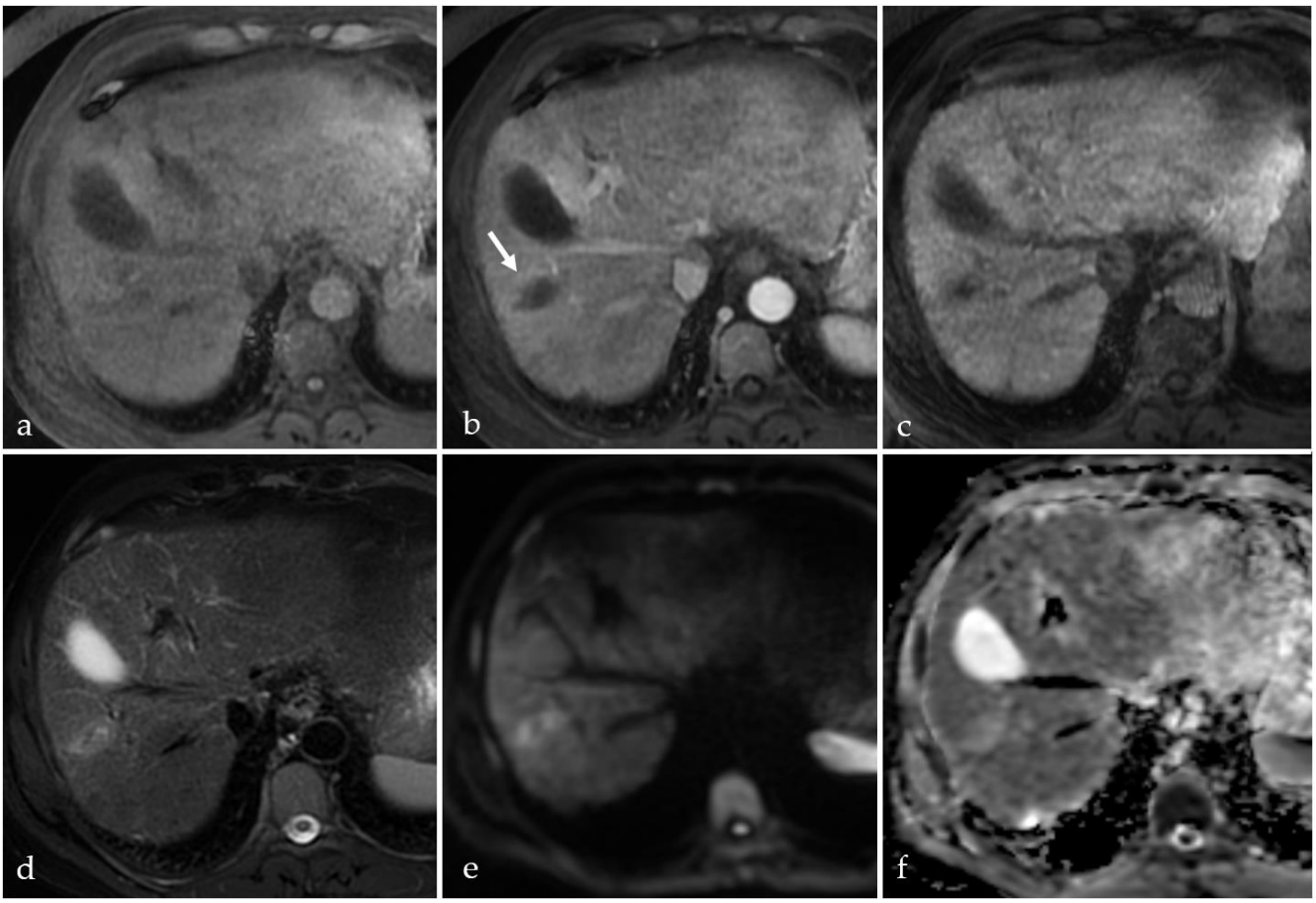

Figure 4. MRI 5 weeks after laser ablation of an HCC nodule in the right liver lobe. The treated nodule (arrow) is isointense on T1 fat sat (**a**), hyperintense on T2 fat sat (**d**), has no arterial enhancement on the subtraction images (**b**), no restricted diffusion (high signal intensity on both DWI (**e**) and ADC (**f**)) and low contrast uptake on the hepatobiliary phase (**c**).

Literature data regarding the histological effects of laser ablation on either liver explants or animal models is scarce. However, follow-up imaging studies describe similar findings to other thermal ablative therapies such as RFA and MWA [49,50]. Ultrasound examination in the days following LA reveals a central zone of vaporization surrounded by a thin halo of carbonization and a peripheral thick rim of coagulation [45].

Coagulation necrosis is the desired effect and its volume depends on the energy delivered [51]. Incomplete or partial necrosis may be observed in a variety of cases such as tumor subtype, growth pattern, and nodule size [52,53]. Moreover, in vivo animal studies showed LA-induced heat stress-related apoptosis in HCC cells as well as hepatocytes via caspase-3/7 activation [54]. Interestingly, new information suggests that laser ablation might stimulate HCC growth due to heat stress via PI3K/mTOR/AKT signaling [55]. These data must be further analyzed and should also be sought in other thermal ablative methods.

2.1.4. High-Intensity Focused Ultrasound

High-intensity focused ultrasound (HIFU) is based on the transmission of mechanical waves emitted by piezoelectric transducers and focused through acoustic lenses; the ultrasounds are emitted at a low frequency (0.8–1.6 MHz) on a specific target [56]. Single or multi-focal HCC disease may be addressed through this method, though success rates with complete ablation are reported in 50 to 100% of cases [57,58]. Data on the improvement in

survival are scarce, and studies on the application of HIFU in HCC generally yield small populations. One of the major advantages of HIFU is that it does not require puncturing the tumor [59] and the heat is quickly generated so dissipation through blood vessels is negligible [23]; however, in order to optimize the ultrasound transmission window, several invasive gestures may be applied, such as rib removal, instillation of saline solution in the pleura or peritoneal cavity, or filling the lumina of the stomach or colon [56]. Conversely, the method might prove useful in patients with advanced liver disease and ascites where other minimally invasive procedures are not indicated.

The effects of HIFU are mixed, and include both thermal and mechanical effects. Thermal effects are caused by the ultrasound energy that raises the temperature and induces coagulative necrosis. Excessive temperatures may be obtained and vaporization may also be achieved through this method [60]. The mechanical effects are represented by acoustic cavitation, a process that implies the creation of microbubbles that subsequently expand and implode, inducing extreme pressure variations that injure the adjacent cells, a process called the "popcorn effect" [60].

HIFU has been deemed safe and effective in ablating small HCC by various studies; despite this, it may face difficulties when attempting the treatment of nodules in areas of the liver that require interventions to optimize acoustic transmission [57,58,61].

2.1.5. Cryoablation

Cryoablation (CA) uses the Joule–Thomson effect to cool the area of ablation by releasing high-pressure argon gas through a cryoprobe [62]. This leads to the formation of an iceball at temperatures below −150 °C that is subsequently thawed [63]. Although cryoablation is not widely used, a randomized controlled trial has shown that 97% of HCC patients undergoing cryoablation had no tumor progression 1 year after the procedure and the overall survival rate at 5 years was 40% [64]. One of the advantages of cryoablation is that real-time observation of the ablated area may be performed through imaging methods, such as CT or US [65]. Technical success is considered when the iceball is at least 5 mm larger than the nodule in any direction [65]. However, small ablation volumes may be achieved with ease using CA in the case of small tumor nodules [66].

CA is effective through two distinct mechanisms. On the one hand, it has direct effects on tumor tissue by forming ice crystals in the intra- and extracellular space as well as an increase in osmotic pressure, causing cell destruction and irreversible damage to cell organelles [24,63]. Then, during thawing, the ice crystals converge into larger ones that further advance cellular injuries; moreover, due to osmotic pressure, water is displaced towards the intracellular space, expanding it and rupturing the cell membrane [63]. On the other hand, the indirect effects relate to the altering of blood flow towards the tumor due to damage to the endothelium of adjacent vessels. This leads to blood vessel thrombosis causing ischemia and cell death in the tributary volume of the vessel [24,46]. A "cold sink" effect was described in CA, and therefore lesions near larger blood vessels may be more difficult to treat.

Cryobiology has studied the effects of CA on living tissue and has shown that freezing triggers an anti-tumor response causing a T-cell response to the tumor [67,68]. This effect, labeled "cryoimmunology", is a secondary advantage to using this ablative technique and the mechanisms involved are still being investigated.

2.2. Non-Thermal Ablative Therapies

Non-thermal ablative therapies rely on various mechanisms to achieve tumor destruction. An overview of the principles is presented in Figure 5.

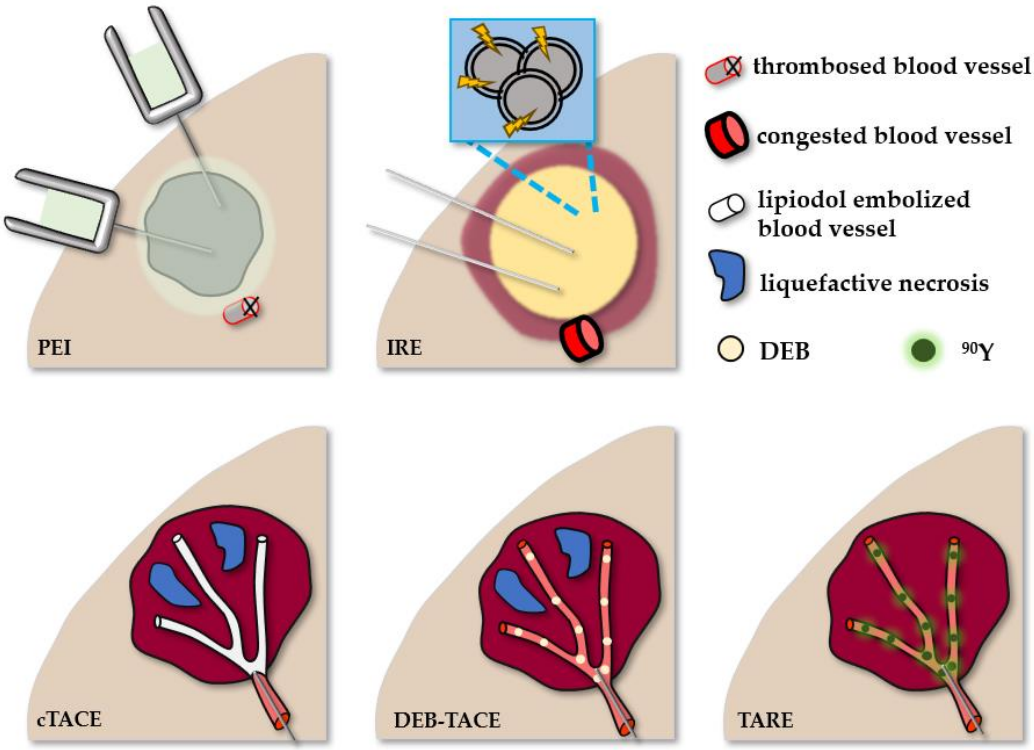

Figure 5. Overview of the non-thermal ablative therapies and their effects. PEI = percutaneous ethanol injection; IRE = irreversible electroporation; cTACE = conventional transarterial chemoembolization; DEB-TACE = drug eluting beads transarterial chemoembolization; TARE = transarterial radioembolization. DEB = drug eluting beads. ^{90}Y = Yttrium-90 microshperes. Additional panel in IRE shows disruption of cellular membranes.

2.2.1. Percutaneous Ethanol Injection

Percutaneous Ethanol Injection (PEI) was demonstrated to be an effective method in treating HCC nodules smaller than 3 cm in diameter, with an initial complete response of up to 96% and 5-year survival rates of up to 63% in patients with smaller tumors [69]. The injection is generally performed under local anesthesia with US guidance and is repeated in various areas of the nodule until it appears hyperechoic, due to the microbubbles in the solution [70]. Due to the lack of standardization regarding the number and location of the injections, as well as injected quantity and rate, some variance in effectiveness may be observed.

After injection, ethanol diffuses into the cells, causing dehydration and protein denaturation leading to coagulation necrosis [71] (Figure 6). The area of necrosis extends around the injection site and should be observed to reach the periphery of the nodule in order to obtain complete ablation. Repeated injections might be necessary in order to improve efficacy, and stronger substances with a higher infiltrative effect are also in use [72]. In patients with liver cirrhosis, ethanol diffuses with ease in the tumor nodule due to it being relatively soft compared to the hardened adjacent liver parenchyma [73]. Ethanol causes endothelial damage and subsequent thrombosis of the feeding vessels, leading to ischemia in the tumor nodule [74]. Animal studies have shown that necrosis can be observed on the needle track when doses higher than 0.3 mL/kg bodyweight are used; also, a fibroblastic reaction occurs in the periphery of the injected area, and may be observed after 5 to 7 days [75].

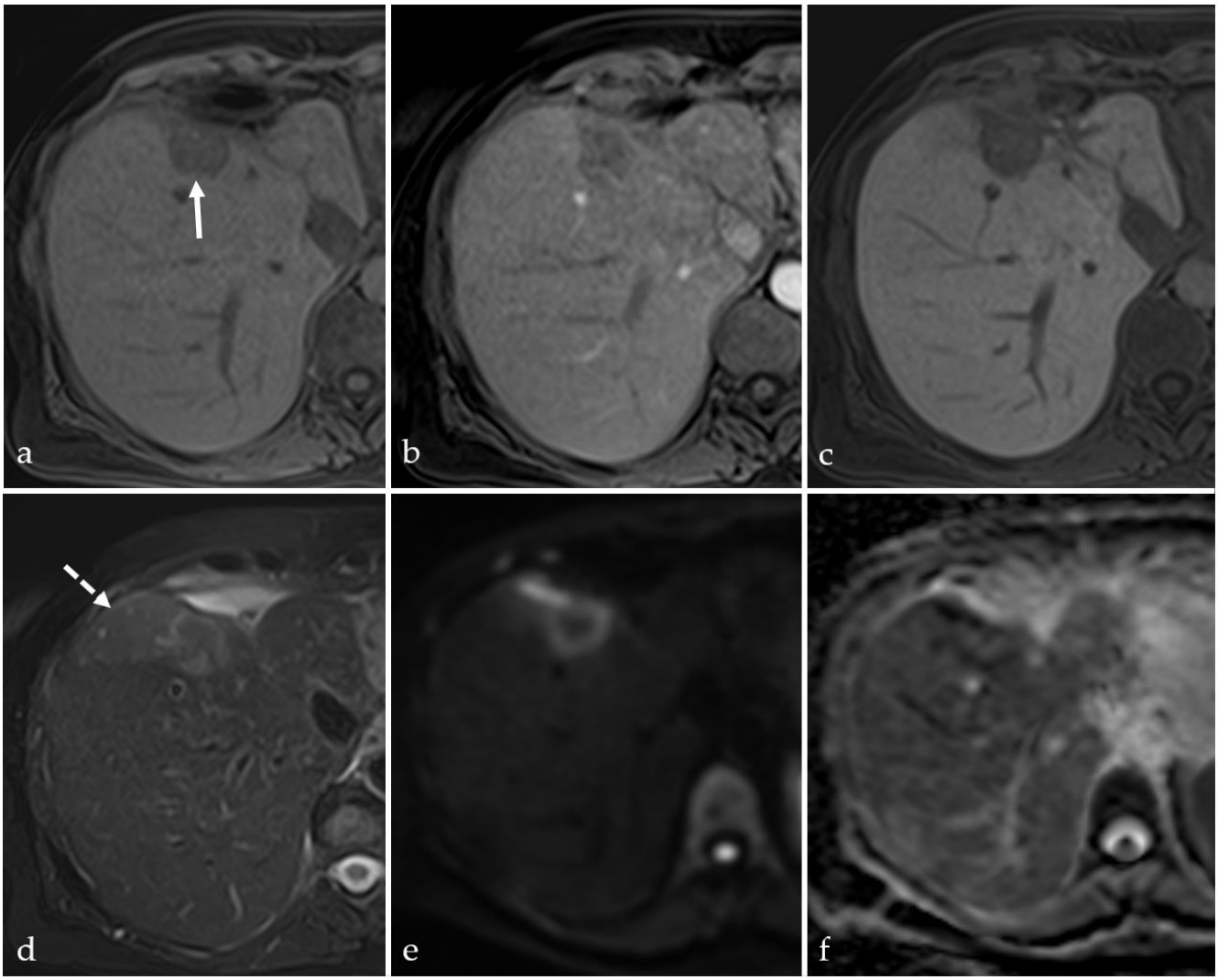

Figure 6. Left hepatectomy and partial right liver lobe resection. MRI examination of a patient who underwent PEI for an HCC nodule (arrow) in the liver segment VIII 5 months prior. The treated nodule has no contrast enhancement in the arterial (**b**) or hepatobiliary (**c**) phase, has low signal intensity on both T1 (**a**) and T2 (**d**) fat saturated images, has peripheral restricted diffusion (**e**,**f**), and an adjacent wedge-shaped area of hypoperfusion (dotted arrow).

The effectiveness of PEI in causing blood vessel occlusion favored its use alongside other ablative techniques such as RFA, where the heat sink effect is diminished, therefore improving the therapeutic success [74].

2.2.2. Irreversible Electroporation

Irreversible electroporation (IRE) is a relatively new, non-thermal therapeutic method for HCC in patients with nodules that usually measure less than 3 cm. IRE is usually reserved for patients that cannot be treated with other minimally invasive methods due to the nodule depth or proximity to major vessels [76]. IRE was successful in obtaining complete ablation in over 90% of nodules and prolonging survival [77–79]. From a technical standpoint, the NanoKnife® system, created by AngioDynamics, which is the widely available commercial solution, uses a direct current of low energy but with high voltage (1000–3000 V) that is generated between the inserted electrodes [80]. The 19-gauge electrodes are parallel-inserted with local anesthesia and under US or CT guidance [81].

The application of IRE causes the appearance of minuscule pores in the cellular membranes in random locations within the ablation area [82]. These pores will expand in

size, increasing membrane permeability and ultimately dissolving the membrane while also triggering apoptosis. The procedure seems to be independent of blood flow, hence its application in nodules near blood vessels [82]. The area of ablation is characterized by hemorrhagic necrosis and edema, and apoptosis contributes to the extent of the cell damage [76]. Large blood vessels, bile ducts, and nerves adjacent to the ablation area appear unaffected [83]. However, minor blood vessels may demonstrate vascular congestion [84].

IRE of HCC nodules also triggers an immunological reaction; a recent study has shown that shortly after the application of IRE, an increase in immune cells such as white blood cells, monocytes, neutrophils, and natural killer cells was identified in peripheral blood; a decrease of regulatory T-cells was also noted, signifying that cytotoxic cells are favored and this immune profile might lead to tumor growth restriction [85]. Neutrophil infiltration of the treated region was detected shortly after the procedure [84].

2.2.3. Transarterial Chemoembolization

Transarterial chemoembolization (TACE) is the standard treatment for patients with BCLC stage B and is one of the most widespread and studied therapeutic options for HCC [86]. The method implies a transarterial approach to the liver nodule under fluoroscopic guidance. Conventional TACE (cTACE) uses a lipiodol drug-charged emulsion followed by an embolizing substance (Figure 7), while a separate technique uses drug-eluting beads (DEB) that release a chemotherapeutic agent over longer periods of time [87] (Figure 8). There are numerous reports of outcomes following TACE, and it appears that DEB-TACE provides a better tumor response than cTACE; the complete response, disease stability, and mortality are overall similar between the two techniques [88].

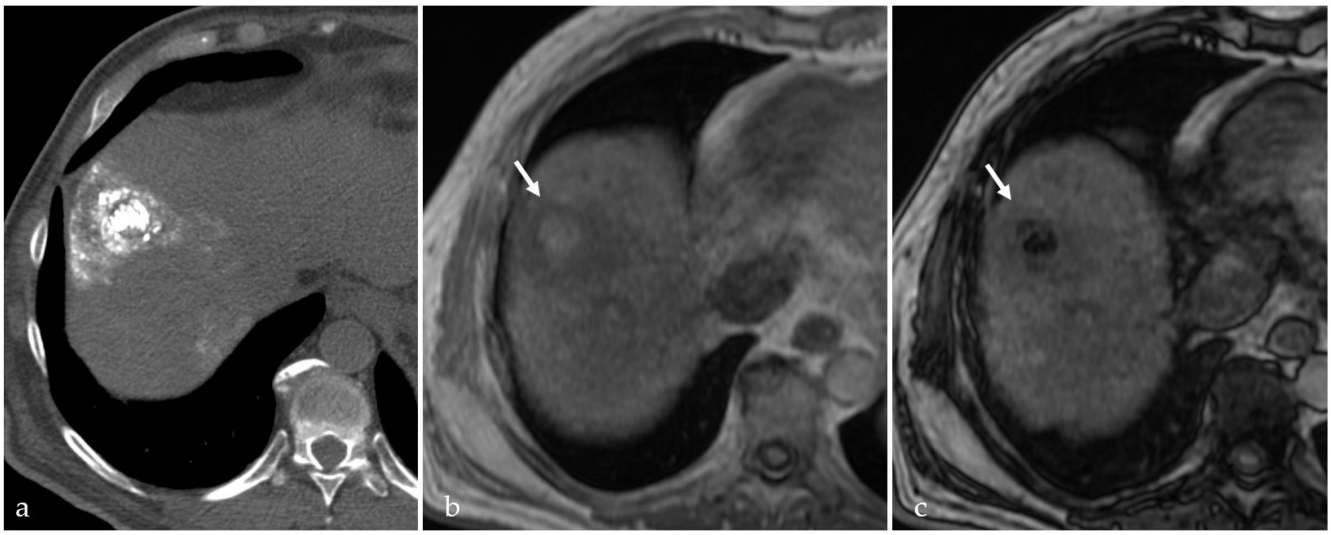

Figure 7. Unenhanced CT scan of a patient with HCC in the right liver lobe, 1 day after cTACE (**a**), and MRI scan of the same patient 5 weeks later (T1 weighted dual echo: "in phase"—(**b**) "out of phase"—(**c**)). The lipiodol used in conventional TACE is hiperdense on CT (**a**), and has signal intensity similar to fat on T1 dual-echo images (arrow)—"in phase" high signal intensity and "out of phase" signal drop.

TACE induces necrosis through a combination of the cytotoxic effect of the injected drugs and the ischemia secondary to the arterial occlusion. The necrosis seems to be greater in supraselective TACE compared to lobar TACE and is directly proportional to the tumor diameter [89]. However, smaller nodules are often hypovascular, a factor negatively affecting the effectiveness of the method [89]. The obtained necrosis is coagulative and is associated with moderate liquefaction and fluid accumulation; infiltration with immune cells may appear in the periphery and areas of cystic changes may be seen after the

treatment of larger nodules [90]. The presence of liquefactive necrosis may favor bacterial infection, therefore antibiotics may be required in larger tumors [91].

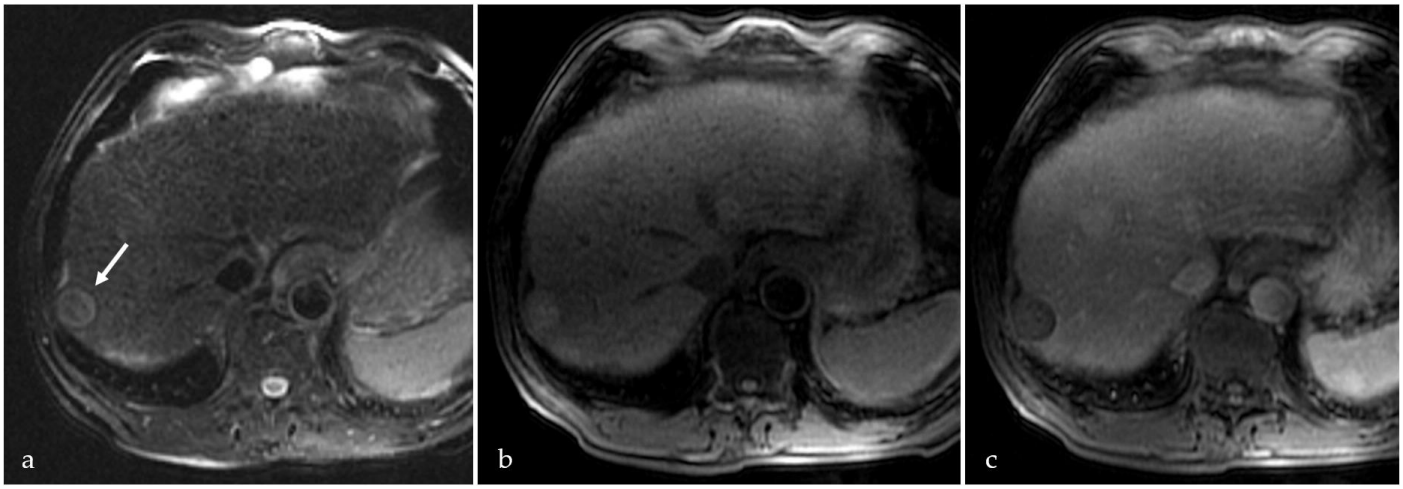

Figure 8. MRI scan of a patient 1 month after DEB-TACE for HCC in liver segments VIII–VII. (**a**)—T2 WI with fat saturation; (**b**)—T1 WI with fat saturation; (**c**)—T1 WI with fat saturation after intravenous contrast. The treated nodule (arrow) is completely necrotic (non-enhancing, (**c**)), with high signal intensity on T2 (**a**) and T1 (**b**), demonstrating both coagulative and liquefactive necrosis.

2.2.4. Yttrium-90 Radioembolization

Yttrium-90 (^{90}Y) transarterial radioembolization (TARE) is performed by injecting the microspheres (20–60 µm in diameter) loaded with the isotope through an endovascular arterial approach [92]. The feeding vessel is not occluded in comparison to cTACE and DEB-TACE; after the injection, the microspheres are taken over by the tumor tissue and emit fatal β-radiation for up to 2 weeks but with a small penetrance (smaller than 3 mm), therefore limiting the negative effects on the healthy hepatocytes [92–94]. ^{90}Y radioembolization has shown objective response rates of up to 88.3% and up to 86.6% overall survival at 3 years [95]. Moreover, ^{90}Y radioembolization appears to be better tolerated than cTACE and yields a longer time to progression of the disease than cTACE [96].

After TARE, the treated nodule may be stationary in size, or show either a decrease or increase in diameter; tumoral size increase usually occurs within the first month and is related to the associated edema and hemorrhage [97]. Therapeutic success is defined as the appearance of coagulative necrosis and usually occurs within the first 4 months [98]. However, transient necrotic areas with a patchy pattern may be seen early after the procedure. Also, a thin and smooth granulation tissue forms around the necrotic area and usually resolves after 4–5 months [97]. Capsular retraction may be seen in nodules closer to the liver surface and is considered a consequence of the fibrosis secondary to the radiation [97,99].

A summary of the advantages, limitations, and performance of the thermal and non-thermal ablative therapies is provided in Table 1.

Table 1. Overview of the minimally invasive treatments for HCC [46,47,63,73,100–111].

Ablative Method	BCLC Stage	Advantages	Limitations	Histological (Imaging) Result	Overall Survival at 5 Years
Thermal ablative methods					
RFA	0-A	Better control for larger nodules	Not recommended for superficial or near-hilum lesions Heat sink effect	Coagulation necrosis (H-iso T1, hT2)	40–68%
MWA	0-A	Higher ablation volume Minimal heat sink effect	Ablation volume may be difficult to estimate More complications in larger nodules	Coagulation necrosis (H-iso T1, hT2)	50–60%
LA	0-A	Better control for larger nodules Better accessibility to nodules	Relatively small zone of ablation, requiring multiple fibers to achieve sufficient volume	Coagulation necrosis (H-iso T1, hT2)	15–34%
HIFU	0-A	Minimal heat sink effect Less invasive	Possible damage to adjacent structures Longer procedure time	Coagulation necrosis (H-iso T1, hT2)	15–60%
CA	0-A	Less painful Area of CA visible on CT/MRI	Cryoshock syndrome is a possible complication	Coagulation necrosis (H-iso T1, hT2)	23–59%
Non-thermal ablative methods					
PEI	0-A	Simple, cheap, accessible	Risk of local progression Difficulty to obtain safety margins	Coagulation necrosis (H-iso T1, hT2)	up to 47%
IRE	0-A	No heat sink effect Applicable to near-hilum lesions	Possible technical difficulty in needle positioning Cardiac gating is required	Coagulation necrosis (H-iso T1, hT2)	14–56%
cTACE	0-B	Combination of local chemotherapy and tumor devascularization	Vascular or biliary complications may occur Difficult in anatomical variants Postembolization syndrome may occur Poor response in hypovascular nodules	Coagulation and liquefactive necrosis (H- and hT1, H- and hT2)	24–54%
DEB-TACE	0-B	Superior chemotherapeutic effect Fewer adverse effects related to the chemotherapeutic drugs		Coagulation and liquefactive necrosis (H- and hT1, H- and hT2)	33–61%
TARE	0-B	Increased radiation dose with curative effect	Radiation-related hepatitis	Coagulation necrosis (H-iso T1, hT2)	up to 40%

RFA = radiofrequency ablation, MWA = microwave ablation, LA = laser ablation, HIFU = high-intensity focused ultrasound; CA = cryoablation; PEI = percutaneous ethanol injection; IRE = irreversible electroporation; cTACE = conventional transarterial chemoembolization; DEB-TACE = drug eluting beads transarterial chemoembolization; TARE = transarterial radioembolization; H = hyperintensity, iso = isointensity; h = hypointensity.

3. Imaging in the Follow-Up of Treated HCC

3.1. Considerations on the MRI Scanning Protocol in HCC Follow-Up

Although each imaging center is free to use a protocol that makes the best use of their MRI machine and equipment, and is most useful for image interpretation, during the last years the LI-RADS recommendations have become standard and are widely applied [112–114]. Briefly, the guideline requires T1 in- and out-of-phase images, T2 with or without fat suppression, and 3D thin (less than 5 mm slice thickness) multiphase T1 contrast-enhanced imaging (with unenhanced, late arterial, and portal venous phase) using either gadobenate dimeglumine or gadoxetate disodium with appropriate delayed or transitional and hepatobiliary phases (at approximately 20 min after contrast injection) [12].

Regarding the choice of contrast agent, some authors showed that gadoxetate disodium has superior sensitivity in the diagnosis of HCC, while other studies cite similar lesion-to-liver contrast ratios, therefore yielding similar diagnostic powers [115–118].

Within LI-RADS, it is also suggested that diffusion-weighted imaging (DWI), subtraction imaging, and multiplanar acquisition are considered as optional images. Increasing the flip angle of the late 3D T1 fat saturated images may increase the contrast between the liver parenchyma and the tumoral lesion [119].

DWI brings a well-recognized advantage in the positive and differential diagnosis of tumors. DWI showed superior reliability compared to analysis of the hepatobiliary phase in the detection of small hypovascular HCCs located in the proximity of blood vessels [120]. Calculation of apparent diffusion coefficient (ADC) values may be useful in predicting the therapeutic response, as significantly lower ADC values were associated with poor or incomplete post-TACE tumor responses [121]. Moreover, ADC was shown to predict survival rates after TACE [122]. However, as shown in the previous sections, the treated nodule may show great inhomogeneity due to the variety of physical and biological processes induced by the treatment. Therefore, when measuring average ADC values in the treated nodule, the heterogeneous structure may influence the findings and lead to false results [123].

Subtraction imaging may be particularly useful in discriminating viable tumor tissue from other T1-WI hyperintensities within the treated nodule, such as the peripheral rim occurring after thermal ablation [124]. A high percentage of patients may show hyperintensity on the non-enhanced T1-WI within the ablation zone and subtraction of the unenhanced set of images from the arterial phase images may be crucial in the differential diagnosis [125,126].

3.2. Expected Post-Treatment Imaging Features in the Absence of Viable Tumor Tissue

Coagulative necrosis is defined as the type of cell death secondary to the decrease or complete stop of blood flow. In consequence, contrast-enhanced MRI will show no uptake. The size of the necrosis should be similar to or larger than the tumor nodule when compared to the pre-therapeutic scans. Within the ablated area, MRI depicts heterogeneous T1-WI hyperintense or isointense areas and a relatively low signal intensity on T2-WI [33]. A target appearance may be seen after thermal ablation, where a central area of T2 hyperintensity corresponding to tissue loss is surrounded by a lower T2-WI intensity and higher T1-WI hyperintense concentric area represented by the coagulation necrosis; the latter may itself be surrounded by a third area of T2-WI hyperintensity with T1-WI isointensity [30]. These target areas evolve with a signal drop in T1-WI in the coagulative necrosis area, while the third concentric area might develop contrast enhancement due to the infiltration by inflammatory cells and may grow thicker over time, while the coagulative necrosis decreases in size [30]. It is commonly accepted that these MRI features of the necrosis are similar in RFA and MWA.

After HIFU-treated HCC, it was reported that a discrepancy between the predicted ablation area and the area identified by MRI may occur, the latter being almost half of the expected size [127]. There is a paucity of studies regarding the MRI features after HIFU due to the limited application of this method.

MRI imaging features after CA are similar to findings after RFA or MWA. Generally, in the days after the procedure, the ablation zone appears hypointense in T1-WI and hyperintense in T2-WI, with heterogeneous areas represented by focal hemorrhage [128]. If large vessels are not punctured, the bleeding is small and evolves in the weeks after the procedure; it can be identified as iso- to hyperintense T1-WI foci and is usually hypointense in T2-WI [129]. The coagulation necrosis appears similar to other thermal ablative procedures; however, a significantly intense T2-WI signal could suggest fluid accumulation within the nodule [129]. A peripheral area of inflammatory response is seen after CA, evolving into fibrosis within the following months. Vascular changes may be identified around the nodule in the form of wedge-shaped areas of increased contrast uptake, which are

produced by the arterial hyperperfusion secondary to portal venous flow reduction [130]. If imaging follow-up is performed at 24 h after the procedure, persistent tumor enhancement may be seen; the contrast uptake is gradual and is thought to be caused by reperfusion through injured vessels within the ablation area [131]. This is specific to cryoablation due to the mechanism of inducing the coagulative necrosis. Contrast enhancement after cryoablation within the tumor nodule may be a normal finding if the uptake is less intense and slower than in the adjacent unablated areas, and this usually resolves within the following months [132].

HCC nodules successfully treated with PEI will show iso- or hyperintensity on T1-WI and uniform hypointensity on T2-WI [71]. However, PEI-treated nodules are associated with persistent fan-shaped T2-hyperintense areas in the vicinity caused by perfusion abnormalities; this was found to be secondary to ethanol infiltration in the peritumoral normal tissues, which caused arterioportal shunts that lasted several months [133]. Additionally, ethanol-related direct toxic effects on healthy liver cells around the treated nodule were identified, causing coagulative necrosis and secondary fibrosis [134]. These T2-hyperintense areas might partly obscure the presence of viable tumor tissue, so careful analysis of these areas is recommended [135].

Imaging follow-up after successful HCC treatment with IRE may show features distinctive to those after thermal ablations. More specifically, persistent contrast enhancement may be seen in the absence of tumor tissue within the ablation zone in the peritumoral liver parenchyma [136]. This may make it difficult to properly assess the ablation area; however, the necrotic area should not present enhancement if no viable tissue is present. An animal study has shown that using IR-prepared images can help delineate a central area of IRE and a peripheral area of reversible electroporation [137]. The same study concluded that temporary contrast enhancement is possible in the IRE zone due to the formation of membrane pores that permitted the uptake of the contrast agent, as well as in the reversible electroporation zone, where the contrast persists in the intracellular space due to electrotransfer [138].

Nodules treated with ^{90}Y present specific MRI findings. The peripheral rim often seen around the area of necrosis due to granulation tissue developing adjacent to the coagulative necrosis can measure up to 5 mm after ^{90}Y; after thermal ablative techniques, a thickness of around 1 mm is expected [139]. This is considered to appear due to the effect of radiation emitted in the peripheral vessels and may be seen for up to 6 months after the procedure [140,141]. Small areas of contrast enhancement may be identified within the ^{90}Y treated nodule and should be monitored unless they are larger than 5 mm, when it is considered to be viable tissue [98].

3.3. Transient Hyperemia

Transient hyperemia is usually visualized as a T2-WI hyperintense rim; the rim might show contrast enhancement, and corresponds to a hemorrhagic area within the congested sinusoid vessels that surround the necrosis [30]. This may be seen in most local regional therapies due to the extension of the aggressive factor (heat, cold, radiation) beyond the treated margins (Figure 9). On DWI, this rim may appear hyperintense with corresponding hypointensity on the ADC map due to the associated cytotoxic edema [142]. Transient hyperemia usually resolves within 6 months when the agent is long-lasting, such as ^{90}Y microspheres, or sooner if the effects are limited to the procedure event [143–145].

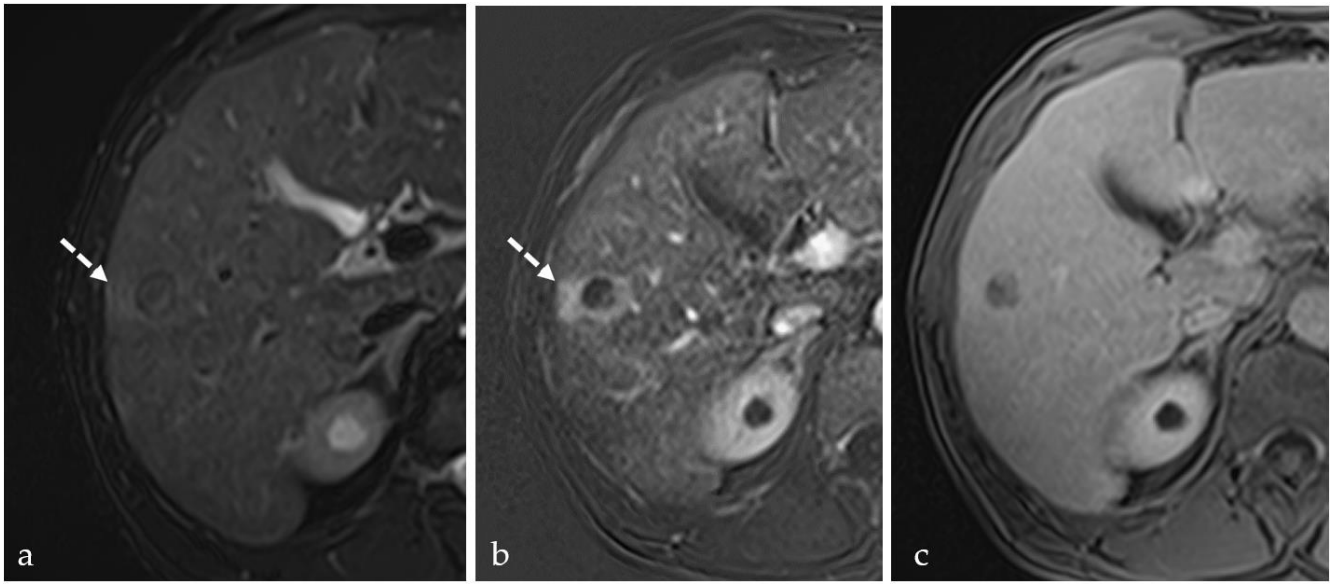

Figure 9. MRI scan: (**a**)—T2 weighted with fat suppression; (**b**)—subtraction; (**c**)—T1 weighted with fat suppression after contrast injection, in the portal venous phase. Transient hyperemia (dotted arrow in (**a**) and (**b**)) surrounding an HCC tumor treated using DEB-TACE. The hyperemia appears as a halo with hazy contour and discrete high signal intensity on T2 WI, arterial phase wash-in, but without portal venous phase wash-out (differentiating it from tumor tissue).

3.4. TACE-Associated Necrosis

As previously mentioned, due to its complex therapeutic mechanisms, TACE may induce a mix of coagulative and liquefactive necrosis. Coagulative necrosis shows a typical T2-WI hypointensity. However, T2-WI focal hyperintensities may be seen when hemorrhage, inflammation, or liquefactive necrosis are associated [146]. Furthermore, after TACE, HCC nodules commonly show variable unenhanced T1-WI intensity, a combined effect of areas of hyperintense hemorrhage and hypointense necrosis [147]. The lipiodol used in cTACE also appears hyperintense on T1-WI in the days following the procedure and increases the contrast-to-noise ratio (CNR); however, it appears that T2-WI is not affected by lipiodol [148]. The extent of lipiodol uptake within the tumor nodule is considered to correlate with therapeutic success [149]. However, this is easily assessed through CT due to the composition of iodine. MRI is not an equally reliable instrument in this regard, although gradient echo images can provide good approximation [150]. Therefore, volumetric techniques have been developed for the prediction of cTACE-induced necrosis extension using MRI contrast enhancement and CT lipiodol volume measurements [151].

DWI also plays an important role in the post-therapeutic assessment of cTACE. Highly vascularized lesions will show prominent restricted diffusion with lower values on the ADC map. This will likely correlate with better results of the TACE [152]. However, necrotic tumors will likely show higher values on the ADC map, which may lead to a poorer prognosis and correlate with higher aggressiveness [153,154]. Regarding DEB-TACE, DWI proved to be useful in predicting treatment response, as increases in ADC after the procedure correlate with longer survival [155].

3.5. Post-Treatment Imaging Features of Tumor Viability

According to LI-RADS, tumor viability is defined as a nodular or thick concentric lesion that either presents contrast wash-in, wash-out, or contrast dynamics similar to pretherapeutic imaging examinations [12] However, viable tumor tissue after treatment can take on different forms (Figure 10).

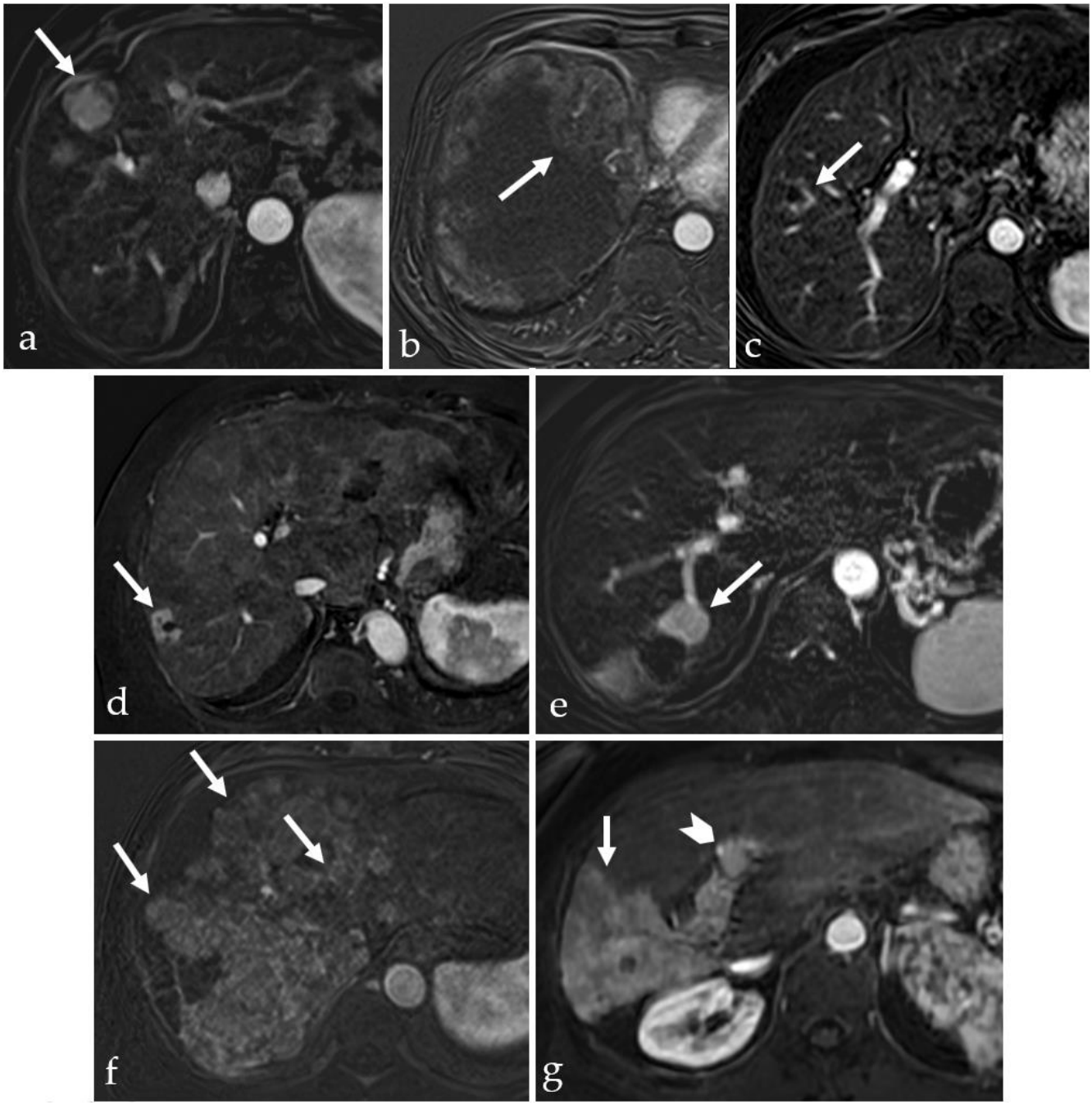

Figure 10. MRI axial images obtained by subtracting a T1 fat saturated image without contrast enhancement from a T1 fat saturated image with contrast enhancement in the arterial phase (**a**–**g**). Persistent/recurrent tumor tissue is hypervascular and can have different shapes: It can be similar to pretreatment (failure of treatment, arrow in (**a**)); Peripheral, inside the treated nodule (incomplete treatment, arrow in (**b**)); Crescent-shaped (arrow in (**c**)); Asymmetric ring (arrow in (**d**)); Nodular-shaped (arrow in (**e**)); Multinodular-shaped (arrows in (**f**)); or wedge-shaped (arrow in (**g**)) with vascular invasion (chevron in (**g**)).

However, there are several distinctive features and recurrence profiles of interest to radiologists and clinicians alike. Hypovascular recurrences can be identified after treatment and their imaging features may be different than the original more vascularized primary tumor [156]. While it is commonly accepted that hypervascularization of a recurrence is an additional risk factor and that hypervascular primary nodules are associated with a poorer

prognosis, it is uncertain how to interpret and manage hypovascular recurrences, especially due to their rarity [157,158]. Another notable HCC subtype is nodule-in-nodule, which is regarded as a morphological marker of early HCC dedifferentiation [159,160]. While, apparently, the prognosis of patients with this unique subtype is better than the "conventional" appearance, knowledge of the imaging features and aspects at post-therapeutic follow-up is essential for correctly identifying tumor recurrence [5,161].

3.6. Current and Future Perspectives in Targeting Tumor Nodules

Considering the advent of minimally invasive procedures and liver surgery for HCC, augmented reality training is gaining interest as an instrument that can aid the interventional radiologist or surgeon [162,163]. The technology can overlay preoperative imaging onto the surgical field and can increase the spatial awareness, reducing risks related to critical adjacent structures or anatomical variations [164,165]. Moreover, integrating image-guided simulation systems in minimally invasive procedures has demonstrated improved patient outcomes, allowing for precise targeting of tumor nodules [166,167].

Looking forward, preoperative planning and additive technologies have an increasingly important role, as 3D-printed anatomical models based on patient-specific imaging can offer the opportunity to plan and practice the procedure with high accuracy [168,169]. Innovations in digital planning as well as augmented reality and artificial intelligence can assist image-guided simulation, can be integrated with surgical robots, and will likely further improve the precision in targeting the tumor nodules while minimizing invasiveness and complications [170–172].

4. Conclusions

Minimally invasive therapies for HCC significantly alter the morphological features of tumor nodules. Each type of therapy induces distinct morphological changes in the treated lesions, such as variations in size, shape, and internal architecture, as well as alterations in contrast enhancement patterns. The proper understanding and interpretation of these imaging characteristics are essential in evaluating treatment efficacy and detecting early signs of recurrence.

Future research perspectives should include the standardization of imaging protocols across different centers in order to consistently identify these morphological features. Advanced imaging techniques, including radiomics and artificial intelligence, offer promising avenues for improving the interpretation of post-treatment imaging features. Moreover, integrating imaging biomarkers with morphological analysis could further enhance the assessment of tumor response and long-term prognosis. Additional research is needed to validate these approaches in larger, multi-institutional studies, which may ultimately lead to personalized treatment strategies for HCC patients.

Author Contributions: Conceptualization, A.-E.S., C.S. and I.G.L.; methodology, A.-E.S. and I.G.L.; formal analysis, S.O.J. and C.S.; writing—original draft preparation, A.-E.S., S.O.J., C.S. and I.G.L.; writing—review and editing, C.S. and I.G.L.; visualization, A.-E.S. and S.O.J.; supervision, I.G.L. All authors have read and agreed to the published version of the manuscript.

Funding: This research received no external funding.

Institutional Review Board Statement: The study was conducted in accordance with the Declaration of Helsinki, and approved by the Ethics Counsil of Fundeni Clinical Institute (number 46648/27 August 2024).

Informed Consent Statement: Informed consent was obtained from all subjects involved in the study.

Data Availability Statement: The data that support the findings of this study are not openly available due to the reasons of sensitivity and are available from the corresponding author upon reasonable request.
Conflicts of Interest: The authors declare no conflicts of interest

.

References

1. McGlynn, K.A.; Petrick, J.L.; El-Serag, H.B. Epidemiology of Hepatocellular Carcinoma. *Hepatology* **2021**, *73* (Suppl. S1), 4–13. [CrossRef] [PubMed]
2. Llovet, J.M.; Kelley, R.K.; Villanueva, A.; Singal, A.G.; Pikarsky, E.; Roayaie, S.; Lencioni, R.; Koike, K.; Zucman-Rossi, J.; Finn, R.S. Hepatocellular carcinoma. *Nat. Rev. Dis. Primers* **2021**, *7*, 6. [CrossRef] [PubMed]
3. Ayuso, C.; Rimola, J.; Vilana, R.; Burrel, M.; Darnell, A.; García-Criado, Á.; Bianchi, L.; Belmonte, E.; Caparroz, C.; Barrufet, M.; et al. Diagnosis and staging of hepatocellular carcinoma (HCC): Current guidelines. *Eur. J. Radiol.* **2018**, *101*, 72–81. [CrossRef] [PubMed]
4. Finn, R.S. The Role of Liver Biopsy in Hepatocellular Carcinoma. *Gastroenterol. Hepatol.* **2016**, *12*, 628–630.
5. Scheau, A.E.; Scheau, C.; Lupescu, I.G. Nodule-in-Nodule Imaging Pattern in Hepatocellular Carcinoma Treated by Transarterial Chemoembolization—A Multiparametric Magnetic Resonance Imaging Study. *J. Gastrointest. Liver Dis.* **2017**, *26*, 387–393. [CrossRef]
6. Wege, H.; Schulze, K.; von Felden, J.; Calderaro, J.; Reig, M. Rare variants of primary liver cancer: Fibrolamellar, combined, and sarcomatoid hepatocellular carcinomas. *Eur. J. Med. Genet.* **2021**, *64*, 104313. [CrossRef]
7. Huang, S.C.; Liao, S.H.; Su, T.H.; Jeng, Y.M.; Kao, J.H. Clinical manifestations and outcomes of patients with scirrhous hepatocellular carcinoma. *Hepatol. Int.* **2021**, *15*, 472–481. [CrossRef]
8. Nevola, R.; Ruocco, R.; Criscuolo, L.; Villani, A.; Alfano, M.; Beccia, D.; Imbriani, S.; Claar, E.; Cozzolino, D.; Sasso, F.C.; et al. Predictors of early and late hepatocellular carcinoma recurrence. *World J. Gastroenterol.* **2023**, *29*, 1243–1260. [CrossRef]
9. European Association for the Study of the Liver. EASL Clinical Practice Guidelines: Management of hepatocellular carcinoma. *J. Hepatol.* **2018**, *69*, 182–236. [CrossRef]
10. Marrero, J.A.; Kulik, L.M.; Sirlin, C.B.; Zhu, A.X.; Finn, R.S.; Abecassis, M.M.; Roberts, L.R.; Heimbach, J.K. Diagnosis, Staging, and Management of Hepatocellular Carcinoma: 2018 Practice Guidance by the American Association for the Study of Liver Diseases. *Hepatology* **2018**, *68*, 723–750. [CrossRef]
11. Singal, A.G.; Llovet, J.M.; Yarchoan, M.; Mehta, N.; Heimbach, J.K.; Dawson, L.A.; Jou, J.H.; Kulik, L.M.; Agopian, V.G.; Marrero, J.A.; et al. AASLD Practice Guidance on prevention, diagnosis, and treatment of hepatocellular carcinoma. *Hepatology* **2023**, *78*, 1922–1965. [CrossRef] [PubMed]
12. Chernyak, V.; Fowler, K.J.; Kamaya, A.; Kielar, A.Z.; Elsayes, K.M.; Bashir, M.R.; Kono, Y.; Do, R.K.; Mitchell, D.G.; Singal, A.G.; et al. Liver Imaging Reporting and Data System (LI-RADS) Version 2018: Imaging of Hepatocellular Carcinoma in At-Risk Patients. *Radiology* **2018**, *289*, 816–830. [CrossRef] [PubMed]
13. Reig, M.; Forner, A.; Rimola, J.; Ferrer-Fàbrega, J.; Burrel, M.; Garcia-Criado, Á.; Kelley, R.K.; Galle, P.R.; Mazzaferro, V.; Salem, R.; et al. BCLC strategy for prognosis prediction and treatment recommendation: The 2022 update. *J. Hepatol.* **2022**, *76*, 681–693. [CrossRef] [PubMed]
14. Abdelsalam, M.E.; Murthy, R.; Avritscher, R.; Mahvash, A.; Wallace, M.J.; Kaseb, A.O.; Odisio, B.C. Minimally invasive image-guided therapies for hepatocellular carcinoma. *J. Hepatocell Carcinoma* **2016**, *3*, 55–61. [CrossRef]
15. Arora, A.; Kumar, A. Treatment Response Evaluation and Follow-up in Hepatocellular Carcinoma. *J. Clin. Exp. Hepatol.* **2014**, *4*, S126–S129. [CrossRef]
16. Crocetti, L.; Bargellini, I.; Cioni, R. Loco-regional treatment of HCC: Current status. *Clin. Radiol.* **2017**, *72*, 626–635. [CrossRef]
17. Han, K.; Kim, J.H. Transarterial chemoembolization in hepatocellular carcinoma treatment: Barcelona clinic liver cancer staging system. *World J. Gastroenterol.* **2015**, *21*, 10327–10335. [CrossRef]
18. Faivre, S.; Rimassa, L.; Finn, R.S. Molecular therapies for HCC: Looking outside the box. *J. Hepatol.* **2020**, *72*, 342–352. [CrossRef]
19. Liu, D.; Song, T. Changes in and challenges regarding the surgical treatment of hepatocellular carcinoma in China. *Biosci. Trends* **2021**, *15*, 142–147. [CrossRef]
20. Bouda, D.; Lagadec, M.; Alba, C.G.; Barrau, V.; Dioguardi Burgio, M.; Moussa, N.; Vilgrain, V.; Ronot, M. Imaging review of hepatocellular carcinoma after thermal ablation: The good, the bad, and the ugly. *J. Magn. Reson. Imaging* **2016**, *44*, 1070–1090. [CrossRef]
21. Wu, Z.J.; Xie, Y.F.; Chang, X.; Zhang, L.; Wu, H.Y.; Liu, J.B.; Zhang, J.X.; Sun, P. Type of Necrosis Influences Prognosis in Hepatocellular Carcinoma After the First Transarterial Chemoembolization. *Med. Sci. Monit.* **2021**, *27*, e929884. [CrossRef] [PubMed]
22. Sindram, D.; Lau, K.N.; Martinie, J.B.; Iannitti, D.A. Hepatic tumor ablation. *Surg. Clin. N. Am.* **2010**, *90*, 863–876. [CrossRef] [PubMed]
23. Niemeyer, D.J.; Simo, K.A.; Iannitti, D.A.; McKillop, I.H. Ablation therapy for hepatocellular carcinoma: Past, present and future perspectives. *Hepat. Oncol.* **2014**, *1*, 67–79. [CrossRef] [PubMed]
24. Shiina, S.; Tateishi, R.; Arano, T.; Uchino, K.; Enooku, K.; Nakagawa, H.; Asaoka, Y.; Sato, T.; Masuzaki, R.; Kondo, Y.; et al. Radiofrequency ablation for hepatocellular carcinoma: 10-year outcome and prognostic factors. *Am. J. Gastroenterol.* **2012**, *107*, 569–577, quiz 578. [CrossRef] [PubMed]
25. Huang, J.; Yan, L.; Cheng, Z.; Wu, H.; Du, L.; Wang, J.; Xu, Y.; Zeng, Y. A randomized trial comparing radiofrequency ablation and surgical resection for HCC conforming to the Milan criteria. *Ann. Surg.* **2010**, *252*, 903–912. [CrossRef]
26. Feng, K.; Yan, J.; Li, X.; Xia, F.; Ma, K.; Wang, S.; Bie, P.; Dong, J. A randomized controlled trial of radiofrequency ablation and surgical resection in the treatment of small hepatocellular carcinoma. *J. Hepatol.* **2012**, *57*, 794–802. [CrossRef]

27. Crocetti, L.; de Baere, T.; Lencioni, R. Quality improvement guidelines for radiofrequency ablation of liver tumours. *Cardiovasc. Interv. Radiol.* **2010**, *33*, 11–17. [CrossRef]
28. McDermott, S.; Gervais, D.A. Radiofrequency ablation of liver tumors. *Semin Interv. Radiol.* **2013**, *30*, 49–55. [CrossRef]
29. Lencioni, R.; Crocetti, L. Radiofrequency ablation of liver cancer. *Tech. Vasc. Interv. Radiol.* **2007**, *10*, 38–46. [CrossRef]
30. Lee, J.D.; Lee, J.M.; Kim, S.W.; Kim, C.S.; Mun, W.S. MR imaging-histopathologic correlation of radiofrequency thermal ablation lesion in a rabbit liver model: Observation during acute and chronic stages. *Korean J. Radiol.* **2001**, *2*, 151–158. [CrossRef]
31. McGahan, J.P.; Brock, J.M.; Tesluk, H.; Gu, W.Z.; Schneider, P.; Browning, P.D. Hepatic ablation with use of radio-frequency electrocautery in the animal model. *J. Vasc. Interv. Radiol.* **1992**, *3*, 291–297. [CrossRef] [PubMed]
32. Rozenblum, N.; Zeira, E.; Bulvik, B.; Gourevitch, S.; Yotvat, H.; Galun, E.; Goldberg, S.N. Radiofrequency Ablation: Inflammatory Changes in the Periablative Zone Can Induce Global Organ Effects, including Liver Regeneration. *Radiology* **2015**, *276*, 416–425. [CrossRef] [PubMed]
33. Kim, Y.S.; Rhim, H.; Lim, H.K.; Choi, D.; Lee, M.W.; Park, M.J. Coagulation necrosis induced by radiofrequency ablation in the liver: Histopathologic and radiologic review of usual to extremely rare changes. *Radiographics* **2011**, *31*, 377–390. [CrossRef] [PubMed]
34. Poggi, G.; Montagna, B.; Di Cesare, P.; Riva, G.; Bernardo, G.; Mazzucco, M.; Riccardi, A. Microwave ablation of hepatocellular carcinoma using a new percutaneous device: Preliminary results. *Anticancer Res.* **2013**, *33*, 1221–1227.
35. Sun, A.X.; Cheng, Z.L.; Wu, P.P.; Sheng, Y.H.; Qu, X.J.; Lu, W.; Zhao, C.G.; Qian, G.J. Clinical outcome of medium-sized hepatocellular carcinoma treated with microwave ablation. *World J. Gastroenterol.* **2015**, *21*, 2997–3004. [CrossRef]
36. Yin, X.Y.; Xie, X.Y.; Lu, M.D.; Xu, H.X.; Xu, Z.F.; Kuang, M.; Liu, G.J.; Liang, J.Y.; Lau, W.Y. Percutaneous thermal ablation of medium and large hepatocellular carcinoma: Long-term outcome and prognostic factors. *Cancer* **2009**, *115*, 1914–1923. [CrossRef]
37. Wang, T.; Lu, X.-J.; Chi, J.-C.; Ding, M.; Zhang, Y.; Tang, X.-Y.; Li, P.; Zhang, L.; Zhang, X.-Y.; Zhai, B. Microwave ablation of hepatocellular carcinoma as first-line treatment: Long term outcomes and prognostic factors in 221 patients. *Sci. Rep.* **2016**, *6*, 32728. [CrossRef]
38. Simon, C.J.; Dupuy, D.E.; Mayo-Smith, W.W. Microwave ablation: Principles and applications. *Radiographics* **2005**, *25* (Suppl. S1), S69–S83. [CrossRef]
39. Habibollahi, P.; Sheth, R.A.; Cressman, E.N.K. Histological Correlation for Radiofrequency and Microwave Ablation in the Local Control of Hepatocellular Carcinoma (HCC) before Liver Transplantation: A Comprehensive Review. *Cancers* **2020**, *13*, 104. [CrossRef]
40. Gravante, G.; Ong, S.L.; Metcalfe, M.S.; Strickland, A.; Dennison, A.R.; Lloyd, D.M. Hepatic microwave ablation: A review of the histological changes following thermal damage. *Liver Int.* **2008**, *28*, 911–921. [CrossRef]
41. Strickland, A.D.; Clegg, P.J.; Cronin, N.J.; Swift, B.; Festing, M.; West, K.P.; Robertson, G.S.; Lloyd, D.M. Experimental study of large-volume microwave ablation in the liver. *Br. J. Surg.* **2002**, *89*, 1003–1007. [CrossRef] [PubMed]
42. Sato, K.; Nakamura, K.; Hamuro, M.; Sakai, Y.; Nishida, N.; Yamada, R.; Ikura, Y.; Ueda, M.; Inoue, Y. The influence of radiofrequency ablation on hepatic vessels in porcine liver. *Hepato-Gastroenterology* **2005**, *52*, 571–574. [PubMed]
43. Kato, T.; Suto, Y.; Hamazoe, R. Effects of microwave tissue coagulation on the livers of normal rabbits: A comparison of findings of image analysis and histopathological examination. *Br. J. Radiol.* **1996**, *69*, 515–521. [CrossRef] [PubMed]
44. Brace, C.L.; Laeseke, P.F.; Sampson, L.A.; Frey, T.M.; van der Weide, D.W.; Lee, F.T., Jr. Microwave ablation with multiple simultaneously powered small-gauge triaxial antennas: Results from an in vivo swine liver model. *Radiology* **2007**, *244*, 151–156. [CrossRef]
45. Pacella, C.M.; Bizzarri, G.; Magnolfi, F.; Cecconi, P.; Caspani, B.; Anelli, V.; Bianchini, A.; Valle, D.; Pacella, S.; Manenti, G.; et al. Laser thermal ablation in the treatment of small hepatocellular carcinoma: Results in 74 patients. *Radiology* **2001**, *221*, 712–720. [CrossRef]
46. Pacella, C.M.; Francica, G.; Di Lascio, F.M.; Arienti, V.; Antico, E.; Caspani, B.; Magnolfi, F.; Megna, A.S.; Pretolani, S.; Regine, R.; et al. Long-term outcome of cirrhotic patients with early hepatocellular carcinoma treated with ultrasound-guided percutaneous laser ablation: A retrospective analysis. *J. Clin. Oncol.* **2009**, *27*, 2615–2621. [CrossRef]
47. Di Costanzo, G.G.; Francica, G.; Pacella, C.M. Laser ablation for small hepatocellular carcinoma: State of the art and future perspectives. *World J. Hepatol.* **2014**, *6*, 704–715. [CrossRef]
48. Gough-Palmer, A.L.; Gedroyc, W.M. Laser ablation of hepatocellular carcinoma—A review. *World J. Gastroenterol.* **2008**, *14*, 7170–7174. [CrossRef]
49. Adwan, H.; Vogl, T.J.; Balaban, Ü.; Nour-Eldin, N.-E.A. Percutaneous Thermal Ablation Therapy of Hepatocellular Carcinoma (HCC): Microwave Ablation (MWA) versus Laser-Induced Thermotherapy (LITT). *Diagnostics* **2022**, *12*, 564. [CrossRef]
50. Arienti, V.; Pretolani, S.; Pacella, C.M.; Magnolfi, F.; Caspani, B.; Francica, G.; Megna, A.S.; Regine, R.; Sponza, M.; Antico, E.; et al. Complications of Laser Ablation for Hepatocellular Carcinoma: A Multicenter Study. *Radiology* **2008**, *246*, 947–955. [CrossRef]
51. Pacella, C.M.; Bizzarri, G.; Francica, G.; Bianchini, A.; De Nuntis, S.; Pacella, S.; Crescenzi, A.; Taccogna, S.; Forlini, G.; Rossi, Z.; et al. Percutaneous laser ablation in the treatment of hepatocellular carcinoma with small tumors: Analysis of factors affecting the achievement of tumor necrosis. *J. Vasc. Interv. Radiol.* **2005**, *16*, 1447–1457. [CrossRef] [PubMed]
52. Francica, G.; Iodice, G.; Delle Cave, M.; Sarrantonio, R.; Lapiccirella, G.; Molese, V.; Smeraldo, D.; Scarano, F.; De Marino, F. Factors Predicting Complete Necrosis Rate after Ultrasound-Guided Percutaneous Laser Thermoablation of Small Hepatocellular Carcinoma Tumors in Cirrhotic Patients: A Multivariate Analysis. *Acta Radiol.* **2007**, *48*, 514–519. [CrossRef] [PubMed]

53. Morisco, F.; Camera, S.; Guarino, M.; Tortora, R.; Cossiga, V.; Vitiello, A.; Cordone, G.; Caporaso, N.; Di Costanzo, G.G.; group, I.L.C. Laser ablation is superior to TACE in large-sized hepatocellular carcinoma: A pilot case–control study. *Oncotarget* **2018**, *9*, 17483–17490. [CrossRef] [PubMed]
54. Thompson, S.M.; Callstrom, M.R.; Butters, K.A.; Knudsen, B.; Grande, J.P.; Roberts, L.R.; Woodrum, D.A. Heat stress induced cell death mechanisms in hepatocytes and hepatocellular carcinoma: In vitro and in vivo study. *Lasers Surg. Med.* **2014**, *46*, 290–301. [CrossRef]
55. Jondal, D.E.; Thompson, S.M.; Butters, K.A.; Knudsen, B.E.; Anderson, J.L.; Carter, R.E.; Roberts, L.R.; Callstrom, M.R.; Woodrum, D.A. Heat Stress and Hepatic Laser Thermal Ablation Induce Hepatocellular Carcinoma Growth: Role of PI3K/mTOR/AKT Signaling. *Radiology* **2018**, *288*, 730–738. [CrossRef]
56. Diana, M.; Schiraldi, L.; Liu, Y.Y.; Memeo, R.; Mutter, D.; Pessaux, P.; Marescaux, J. High intensity focused ultrasound (HIFU) applied to hepato-bilio-pancreatic and the digestive system-current state of the art and future perspectives. *Hepatobiliary Surg. Nutr.* **2016**, *5*, 329–344. [CrossRef]
57. Zhang, L.; Zhu, H.; Jin, C.; Zhou, K.; Li, K.; Su, H.; Chen, W.; Bai, J.; Wang, Z. High-intensity focused ultrasound (HIFU): Effective and safe therapy for hepatocellular carcinoma adjacent to major hepatic veins. *Eur. Radiol.* **2009**, *19*, 437–445. [CrossRef]
58. Orsi, F.; Zhang, L.; Arnone, P.; Orgera, G.; Bonomo, G.; Vigna, P.D.; Monfardini, L.; Zhou, K.; Chen, W.; Wang, Z.; et al. High-intensity focused ultrasound ablation: Effective and safe therapy for solid tumors in difficult locations. *AJR Am. J. Roentgenol.* **2010**, *195*, W245–W252. [CrossRef]
59. Hutchinson, L. HIFU is effective for unresectable HCC. *Nat. Rev. Clin. Oncol.* **2011**, *8*, 385. [CrossRef]
60. Mearini, L. High intensity focused ultrasound, liver disease and bridging therapy. *World J. Gastroenterol.* **2013**, *19*, 7494–7499. [CrossRef]
61. Tsang, S.H.; Ma, K.W.; She, W.H.; Chu, F.; Lau, V.; Lam, S.W.; Cheung, T.T.; Lo, C.M. High-intensity focused ultrasound ablation of liver tumors in difficult locations. *Int. J. Hyperth.* **2021**, *38*, 56–64. [CrossRef] [PubMed]
62. Mahnken, A.H.; König, A.M.; Figiel, J.H. Current Technique and Application of Percutaneous Cryotherapy. *RöFo—Fortschr. Geb. Röntgenstrahlen Bildgeb. Verfahr.* **2018**, *190*, 836–846. [CrossRef]
63. Niu, L.Z.; Li, J.L.; Xu, K.C. Percutaneous Cryoablation for Liver Cancer. *J. Clin. Transl. Hepatol.* **2014**, *2*, 182–188. [CrossRef] [PubMed]
64. Wang, C.; Wang, H.; Yang, W.; Hu, K.; Xie, H.; Hu, K.Q.; Bai, W.; Dong, Z.; Lu, Y.; Zeng, Z.; et al. Multicenter randomized controlled trial of percutaneous cryoablation versus radiofrequency ablation in hepatocellular carcinoma. *Hepatology* **2015**, *61*, 1579–1590. [CrossRef] [PubMed]
65. Orlacchio, A.; Bazzocchi, G.; Pastorelli, D.; Bolacchi, F.; Angelico, M.; Almerighi, C.; Masala, S.; Simonetti, G. Percutaneous cryoablation of small hepatocellular carcinoma with US guidance and CT monitoring: Initial experience. *Cardiovasc. Interv. Radiol.* **2008**, *31*, 587–594. [CrossRef]
66. McWilliams, J.P.; Yamamoto, S.; Raman, S.S.; Loh, C.T.; Lee, E.W.; Liu, D.M.; Kee, S.T. Percutaneous ablation of hepatocellular carcinoma: Current status. *J. Vasc. Interv. Radiol.* **2010**, *21*, S204–S213. [CrossRef]
67. Hoffmann, N.E.; Coad, J.E.; Huot, C.S.; Swanlund, D.J.; Bischof, J.C. Investigation of the mechanism and the effect of cryoimmunology in the Copenhagen rat. *Cryobiology* **2001**, *42*, 59–68. [CrossRef]
68. Sabel, M.S. Cryo-immunology: A review of the literature and proposed mechanisms for stimulatory versus suppressive immune responses. *Cryobiology* **2009**, *58*, 1–11. [CrossRef]
69. Sala, M.; Llovet, J.M.; Vilana, R.; Bianchi, L.; Solé, M.; Ayuso, C.; Brú, C.; Bruix, J. Initial response to percutaneous ablation predicts survival in patients with hepatocellular carcinoma. *Hepatology* **2004**, *40*, 1352–1360. [CrossRef]
70. Branco, F.; Brú, C.; Vilana, R.; Bianchi, L.; Alves de Mattos, A. Percutaneous ethanol injection before liver transplantation in the hepatocellular carcinoma. *Ann. Hepatol.* **2009**, *8*, 220–227. [CrossRef]
71. Lee, M.J.; Mueller, P.R.; Dawson, S.L.; Gazelle, S.G.; Hahn, P.F.; Goldberg, M.A.; Boland, G.W. Percutaneous ethanol injection for the treatment of hepatic tumors: Indications, mechanism of action, technique, and efficacy. *AJR Am. J. Roentgenol.* **1995**, *164*, 215–220. [CrossRef] [PubMed]
72. Ohnishi, K.; Ohyama, N.; Ito, S.; Fujiwara, K. Small hepatocellular carcinoma: Treatment with US-guided intratumoral injection of acetic acid. *Radiology* **1994**, *193*, 747–752. [CrossRef] [PubMed]
73. Livraghi, T.; Giorgio, A.; Marin, G.; Salmi, A.; de Sio, I.; Bolondi, L.; Pompili, M.; Brunello, F.; Lazzaroni, S.; Torzilli, G.; et al. Hepatocellular carcinoma and cirrhosis in 746 patients: Long-term results of percutaneous ethanol injection. *Radiology* **1995**, *197*, 101–108. [CrossRef] [PubMed]
74. Tan, Y.; Ding, X.; Long, H.; Ye, J.; Huang, T.; Lin, Y.; Lv, M.; Xie, X.; Huang, G. Percutaneous ethanol injection enhanced the efficacy of radiofrequency ablation in the treatment of HCC: An insight into the mechanism of ethanol action. *Int. J. Hyperth.* **2021**, *38*, 1394–1400. [CrossRef]
75. Festi, D.; Monti, F.; Casanova, S.; Livraghi, T.; Frabboni, R.; Roversi, C.A.; Bertoli, D.; Borelli, G.; Mazzella, G.; Bazzoli, F.; et al. Morphological and biochemical effects of intrahepatic alcohol injection in the rabbit. *J. Gastroenterol. Hepatol.* **1990**, *5*, 402–406. [CrossRef]
76. Zimmerman, A.; Grand, D.; Charpentier, K.P. Irreversible electroporation of hepatocellular carcinoma: Patient selection and perspectives. *J. Hepatocell Carcinoma* **2017**, *4*, 49–58. [CrossRef]

77. Scheffer, H.J.; Nielsen, K.; de Jong, M.C.; van Tilborg, A.A.; Vieveen, J.M.; Bouwman, A.R.; Meijer, S.; van Kuijk, C.; van den Tol, P.M.; Meijerink, M.R. Irreversible electroporation for nonthermal tumor ablation in the clinical setting: A systematic review of safety and efficacy. *J. Vasc. Interv. Radiol.* **2014**, *25*, 997–1011, quiz 1011. [CrossRef]
78. Kalra, N.; Gupta, P.; Gorsi, U.; Bhujade, H.; Chaluvashetty, S.B.; Duseja, A.; Singh, V.; Dhiman, R.K.; Chawla, Y.K.; Khandelwal, N. Irreversible Electroporation for Unresectable Hepatocellular Carcinoma: Initial Experience. *Cardiovasc. Interv. Radiol.* **2019**, *42*, 584–590. [CrossRef]
79. Niessen, C.; Thumann, S.; Beyer, L.; Pregler, B.; Kramer, J.; Lang, S.; Teufel, A.; Jung, E.M.; Stroszczynski, C.; Wiggermann, P. Percutaneous Irreversible Electroporation: Long-term survival analysis of 71 patients with inoperable malignant hepatic tumors. *Sci. Rep.* **2017**, *7*, 43687. [CrossRef]
80. Narayanan, G.; Froud, T.; Suthar, R.; Barbery, K. Irreversible electroporation of hepatic malignancy. *Semin Interv. Radiol* **2013**, *30*, 67–73. [CrossRef]
81. Sugimoto, K.; Abe, M.; Yoshimasu, Y.; Takeuchi, H.; Kasai, Y.; Itoi, T. Irreversible electroporation of hepatocellular carcinoma: The role of ultrasonography. *Ultrasonography* **2020**, *39*, 229–237. [CrossRef] [PubMed]
82. Deipolyi, A.R.; Golberg, A.; Yarmush, M.L.; Arellano, R.S.; Oklu, R. Irreversible electroporation: Evolution of a laboratory technique in interventional oncology. *Diagn. Interv. Radiol.* **2014**, *20*, 147–154. [CrossRef] [PubMed]
83. Chen, X.; Ren, Z.; Zhu, T.; Zhang, X.; Peng, Z.; Xie, H.; Zhou, L.; Yin, S.; Sun, J.; Zheng, S. Electric Ablation with Irreversible Electroporation (IRE) in Vital Hepatic Structures and Follow-up Investigation. *Sci. Rep.* **2015**, *5*, 16233. [CrossRef] [PubMed]
84. Belfiore, M.P.; De Chiara, M.; Reginelli, A.; Clemente, A.; Urraro, F.; Grassi, R.; Belfiore, G.; Cappabianca, S. An overview of the irreversible electroporation for the treatment of liver metastases: When to use it. *Front. Oncol.* **2022**, *12*, 943176. [CrossRef]
85. Guo, X.; Du, F.; Liu, Q.; Guo, Y.; Wang, Q.; Huang, W.; Wang, Z.; Ding, X.; Wu, Z. Immunological effect of irreversible electroporation on hepatocellular carcinoma. *BMC Cancer* **2021**, *21*, 443. [CrossRef]
86. Lencioni, R.; Petruzzi, P.; Crocetti, L. Chemoembolization of hepatocellular carcinoma. *Semin Interv. Radiol.* **2013**, *30*, 3–11. [CrossRef]
87. Raoul, J.L.; Forner, A.; Bolondi, L.; Cheung, T.T.; Kloeckner, R.; de Baere, T. Updated use of TACE for hepatocellular carcinoma treatment: How and when to use it based on clinical evidence. *Cancer Treat. Rev.* **2019**, *72*, 28–36. [CrossRef]
88. Bzeizi, K.I.; Arabi, M.; Jamshidi, N.; Albenmousa, A.; Sanai, F.M.; Al-Hamoudi, W.; Alghamdi, S.; Broering, D.; Alqahtani, S.A. Conventional Transarterial Chemoembolization Versus Drug-Eluting Beads in Patients with Hepatocellular Carcinoma: A Systematic Review and Meta-Analysis. *Cancers* **2021**, *13*, 6172. [CrossRef]
89. Golfieri, R.; Cappelli, A.; Cucchetti, A.; Piscaglia, F.; Carpenzano, M.; Peri, E.; Ravaioli, M.; D'Errico-Grigioni, A.; Pinna, A.D.; Bolondi, L. Efficacy of selective transarterial chemoembolization in inducing tumor necrosis in small (<5 cm) hepatocellular carcinomas. *Hepatology* **2011**, *53*, 1580–1589. [CrossRef]
90. Hsu, H.C.; Wei, T.C.; Tsang, Y.M.; Wu, M.Z.; Lin, Y.H.; Chuang, S.M. Histologic assessment of resected hepatocellular carcinoma after transcatheter hepatic arterial embolization. *Cancer* **1986**, *57*, 1184–1191. [CrossRef]
91. Liu, Y.; Wang, Y.; Wei, Z.; Wang, T.; Yang, S.; Xiang, C.; Wang, X.; Gong, L.; Dong, J.; Lu, Q.; et al. Exploratory study of microparticle transcatheter arterial chemoembolization combined with resection for huge hepatocellular carcinoma. *iLIVER* **2022**, *1*, 35–42. [CrossRef]
92. Molvar, C.; Lewandowski, R. Yttrium-90 Radioembolization of Hepatocellular Carcinoma-Performance, Technical Advances, and Future Concepts. *Semin Interv. Radiol.* **2015**, *32*, 388–397. [CrossRef]
93. Sato, K.; Lewandowski, R.J.; Bui, J.T.; Omary, R.; Hunter, R.D.; Kulik, L.; Mulcahy, M.; Liu, D.; Chrisman, H.; Resnick, S.; et al. Treatment of unresectable primary and metastatic liver cancer with yttrium-90 microspheres (TheraSphere): Assessment of hepatic arterial embolization. *Cardiovasc. Interv. Radiol.* **2006**, *29*, 522–529. [CrossRef] [PubMed]
94. Salem, R.; Lewandowski, R.J. Chemoembolization and radioembolization for hepatocellular carcinoma. *Clin. Gastroenterol. Hepatol.* **2013**, *11*, 604–611, quiz e643–604. [CrossRef] [PubMed]
95. Salem, R.; Johnson, G.E.; Kim, E.; Riaz, A.; Bishay, V.; Boucher, E.; Fowers, K.; Lewandowski, R.; Padia, S.A. Yttrium-90 Radioembolization for the Treatment of Solitary, Unresectable HCC: The LEGACY Study. *Hepatology* **2021**, *74*, 2342–2352. [CrossRef]
96. Salem, R.; Gordon, A.C.; Mouli, S.; Hickey, R.; Kallini, J.; Gabr, A.; Mulcahy, M.F.; Baker, T.; Abecassis, M.; Miller, F.H.; et al. Y90 Radioembolization Significantly Prolongs Time to Progression Compared With Chemoembolization in Patients with Hepatocellular Carcinoma. *Gastroenterology* **2016**, *151*, 1155–1163.e1152. [CrossRef]
97. Singh, P.; Anil, G. Yttrium-90 radioembolization of liver tumors: What do the images tell us? *Cancer Imaging* **2014**, *13*, 645–657. [CrossRef]
98. Keppke, A.L.; Salem, R.; Reddy, D.; Huang, J.; Jin, J.; Larson, A.C.; Miller, F.H. Imaging of hepatocellular carcinoma after treatment with yttrium-90 microspheres. *AJR Am. J. Roentgenol.* **2007**, *188*, 768–775. [CrossRef]
99. Atassi, B.; Bangash, A.K.; Bahrani, A.; Pizzi, G.; Lewandowski, R.J.; Ryu, R.K.; Sato, K.T.; Gates, V.L.; Mulcahy, M.F.; Kulik, L.; et al. Multimodality imaging following 90Y radioembolization: A comprehensive review and pictorial essay. *Radiographics* **2008**, *28*, 81–99. [CrossRef]
100. Adwan, H.; Hammann, L.; Vogl, T.J. Microwave Ablation of Recurrent Hepatocellular Carcinoma after Curative Surgical Resection. *J. Clin. Med.* **2023**, *12*, 2560. [CrossRef]

101. Sun, Q.; Shi, J.; Ren, C.; Du, Z.; Shu, G.; Wang, Y. Survival analysis following microwave ablation or surgical resection in patients with hepatocellular carcinoma conforming to the Milan criteria. *Oncol. Lett.* **2020**, *19*, 4066–4076. [CrossRef] [PubMed]
102. Llovet, J.M.; De Baere, T.; Kulik, L.; Haber, P.K.; Greten, T.F.; Meyer, T.; Lencioni, R. Locoregional therapies in the era of molecular and immune treatments for hepatocellular carcinoma. *Nat. Rev. Gastroenterol. Hepatol.* **2021**, *18*, 293–313. [CrossRef] [PubMed]
103. Rong, G.; Bai, W.; Dong, Z.; Wang, C.; Lu, Y.; Zeng, Z.; Qu, J.; Lou, M.; Wang, H.; Gao, X.; et al. Long-Term Outcomes of Percutaneous Cryoablation for Patients with Hepatocellular Carcinoma within Milan Criteria. *PLoS ONE* **2015**, *10*, e0123065. [CrossRef] [PubMed]
104. Sehmbi, A.S.; Froghi, S.; Oliveira de Andrade, M.; Saffari, N.; Fuller, B.; Quaglia, A.; Davidson, B. Systematic review of the role of high intensity focused ultrasound (HIFU) in treating malignant lesions of the hepatobiliary system. *HPB* **2021**, *23*, 187–196. [CrossRef]
105. Frühling, P.; Stillström, D.; Holmquist, F.; Nilsson, A.; Freedman, J. Irreversible electroporation of hepatocellular carcinoma and colorectal cancer liver metastases: A nationwide multicenter study with short- and long-term follow-up. *Eur. J. Surg. Oncol.* **2023**, *49*, 107046. [CrossRef]
106. Liu, Y.-S.; Lin, C.-Y.; Chuang, M.-T.; Lin, C.-Y.; Tsai, Y.-S.; Wang, C.-K.; Ou, M.-C. Five-year outcome of conventional and drug-eluting transcatheter arterial chemoembolization in patients with hepatocellular carcinoma. *BMC Gastroenterol.* **2018**, *18*, 124. [CrossRef]
107. Lee, S.; Jeong, Y.Y.; Lee, B.C.; Shin, S.S.; Heo, S.H.; Kim, H.O.; Park, C.; Jeong, W.G. Drug-Eluting Bead Transarterial Chemoembolization Versus Radiofrequency Ablation as an Initial Treatment of Single Small ($\leq$3 cm) Hepatocellular Carcinoma. *J. Korean Med. Sci.* **2023**, *38*, e362. [CrossRef]
108. Ma, Z.; Zhou, W.; Huang, H.; Yao, Y. Prognosis comparison between hepatocellular carcinoma patients with microvascular invasion who received hepatectomy alone and those who underwent early PA-TACE: A retrospective cohort study. *J. Gastrointest. Oncol.* **2024**, *15*, 1112–1121. [CrossRef]
109. Teyateeti, A.; Mahvash, A.; Long, J.P.; Abdelsalam, M.E.; Avritscher, R.; Chasen, B.; Kaseb, A.O.; Kuban, J.D.; Murthy, R.; Odisio, B.C.; et al. Survival Outcomes for Yttrium-90 Transarterial Radioembolization with and without Sorafenib for Unresectable Hepatocellular Carcinoma Patients. *J. Hepatocell. Carcinoma* **2020**, *7*, 117–131. [CrossRef]
110. Horvat, N.; de Oliveira, A.I.; Clemente de Oliveira, B.; Araujo-Filho, J.A.B.; El Homsi, M.; Elsakka, A.; Bajwa, R.; Martins, G.L.P.; Elsayes, K.M.; Menezes, M.R. Local-Regional Treatment of Hepatocellular Carcinoma: A Primer for Radiologists. *Radiographics* **2022**, *42*, 1670–1689. [CrossRef]
111. Ahmed, M.; Goldberg, S.N. Thermal Ablation Therapy for Hepatocellular Carcinoma. *J. Vasc. Interv. Radiol.* **2002**, *13*, S231–S243. [CrossRef] [PubMed]
112. Khatri, G.; Pedrosa, I.; Ananthakrishnan, L.; de Leon, A.D.; Fetzer, D.T.; Leyendecker, J.; Singal, A.G.; Xi, Y.; Yopp, A.; Yokoo, T. Abbreviated-protocol screening MRI vs. complete-protocol diagnostic MRI for detection of hepatocellular carcinoma in patients with cirrhosis: An equivalence study using LI-RADS v2018. *J. Magn. Reson. Imaging* **2020**, *51*, 415–425. [CrossRef] [PubMed]
113. Basha, M.A.A.; Al Azzazy, M.Z.; Ahmed, A.F.; Yousef, H.Y.; Shehata, S.M.; El Sammak, D.; Fathy, T.; Obaya, A.A.; Abdelbary, E.H. Does a combined CT and MRI protocol enhance the diagnostic efficacy of LI-RADS in the categorization of hepatic observations? A prospective comparative study. *Eur. Radiol.* **2018**, *28*, 2592–2603. [CrossRef] [PubMed]
114. Kamal, O.; Sy, E.; Chernyak, V.; Gupta, A.; Yaghmai, V.; Fowler, K.; Karampinos, D.; Shanbhogue, K.; Miller, F.H.; Kambadakone, A.; et al. Optional MRI sequences for LI-RADS: Why, what, and how? *Abdom. Radiol.* **2023**, *48*, 519–531. [CrossRef] [PubMed]
115. Stocker, D.; Hectors, S.; Bane, O.; Vietti-Violi, N.; Said, D.; Kennedy, P.; Cuevas, J.; Cunha, G.M.; Sirlin, C.B.; Fowler, K.J.; et al. Dynamic contrast-enhanced MRI perfusion quantification in hepatocellular carcinoma: Comparison of gadoxetate disodium and gadobenate dimeglumine. *Eur. Radiol.* **2021**, *31*, 9306–9315. [CrossRef]
116. Zech, C.J.; Schwenke, C.; Endrikat, J. Diagnostic Efficacy and Safety of Gadoxetate Disodium vs Gadobenate Dimeglumine in Patients with Known or Suspected Focal Liver Lesions: Results of a Clinical Phase III Study. *Magn. Reason. Insights* **2019**, *12*, 1178623x19827976. [CrossRef]
117. Tirkes, T.; Mehta, P.; Aisen, A.M.; Lall, C.; Akisik, F. Comparison of Dynamic Phase Enhancement of Hepatocellular Carcinoma Using Gadoxetate Disodium vs Gadobenate Dimeglumine. *J. Comput. Assist. Tomogr.* **2015**, *39*, 479–482. [CrossRef]
118. Allen, B.C.; Ho, L.M.; Jaffe, T.A.; Miller, C.M.; Mazurowski, M.A.; Bashir, M.R. Comparison of Visualization Rates of LI-RADS Version 2014 Major Features with IV Gadobenate Dimeglumine or Gadoxetate Disodium in Patients at Risk for Hepatocellular Carcinoma. *AJR Am. J. Roentgenol.* **2018**, *210*, 1266–1272. [CrossRef]
119. Song, M.; Cho, H.J.; Cho, Y.K.; Kim, M.Y.; Noh, S.I.; Yang, S.H. Detecting hepatocellular carcinoma in gadoxetic-acid-enhanced hepatobiliary-phase MR imaging at 3T: Comparing high and low flip angle. *Jpn. J. Radiol.* **2013**, *31*, 803–811. [CrossRef]
120. Park, M.J.; Kim, Y.K.; Lee, M.W.; Lee, W.J.; Kim, Y.-S.; Kim, S.H.; Choi, D.; Rhim, H. Small Hepatocellular Carcinomas: Improved Sensitivity by Combining Gadoxetic Acid–enhanced and Diffusion-weighted MR Imaging Patterns. *Radiology* **2012**, *264*, 761–770. [CrossRef]
121. Mannelli, L.; Kim, S.; Hajdu, C.H.; Babb, J.S.; Taouli, B. Serial diffusion-weighted MRI in patients with hepatocellular carcinoma: Prediction and assessment of response to transarterial chemoembolization. Preliminary experience. *Eur. J. Radiol.* **2013**, *82*, 577–582. [CrossRef] [PubMed]

122. Corona-Villalobos, C.P.; Halappa, V.G.; Bonekamp, S.; Eng, J.; Reyes, D.; Cosgrove, D.; Rastegar, N.; Pan, L.; Pawlik, T.M.; Kamel, I.R. Functional magnetic resonance imaging response of targeted tumor burden and its impact on survival in patients with hepatocellular carcinoma. *Investig. Radiol.* **2015**, *50*, 283–289. [CrossRef] [PubMed]
123. Gluskin, J.S.; Chegai, F.; Monti, S.; Squillaci, E.; Mannelli, L. Hepatocellular Carcinoma and Diffusion-Weighted MRI: Detection and Evaluation of Treatment Response. *J. Cancer* **2016**, *7*, 1565–1570. [CrossRef] [PubMed]
124. Dromain, C.; de Baere, T.; Elias, D.; Kuoch, V.; Ducreux, M.; Boige, V.; Petrow, P.; Roche, A.; Sigal, R. Hepatic tumors treated with percutaneous radio-frequency ablation: CT and MR imaging follow-up. *Radiology* **2002**, *223*, 255–262. [CrossRef] [PubMed]
125. Gabr, A.E.; Mikhael, H.S.W.; El-Maadawy, S.M. Comparison between subtraction and dynamic MRI in assessing treatment response following radiofrequency ablation in patients with hepatocellular carcinoma. *Egypt. J. Radiol. Nucl. Med.* **2021**, *52*, 285. [CrossRef]
126. El-Assaly, H.; Abdallah, M.F.H.; Mohamed, W.M.; Youssef, M.I. Additive role of dynamic subtraction MRI in assessment of unresolved HCC post-radiofrequency ablation. *Egypt. J. Radiol. Nucl. Med.* **2021**, *52*, 257. [CrossRef]
127. Illing, R.O.; Kennedy, J.E.; Wu, F.; ter Haar, G.R.; Protheroe, A.S.; Friend, P.J.; Gleeson, F.V.; Cranston, D.W.; Phillips, R.R.; Middleton, M.R. The safety and feasibility of extracorporeal high-intensity focused ultrasound (HIFU) for the treatment of liver and kidney tumours in a Western population. *Br. J. Cancer* **2005**, *93*, 890–895. [CrossRef]
128. Gatti, M.; Maino, C.; Darvizeh, F.; Serafini, A.; Tricarico, E.; Guarneri, A.; Inchingolo, R.; Ippolito, D.; Ricardi, U.; Fonio, P.; et al. Role of gadoxetic acid-enhanced liver magnetic resonance imaging in the evaluation of hepatocellular carcinoma after locoregional treatment. *World J. Gastroenterol.* **2022**, *28*, 3116–3131. [CrossRef]
129. Ratanaprasatporn, L.; Sainani, N.; Duda, J.B.; Aghayev, A.; Tatli, S.; Silverman, S.G.; Shyn, P.B. Imaging findings during and after percutaneous cryoablation of hepatic tumors. *Abdom. Radiol.* **2019**, *44*, 2602–2626. [CrossRef]
130. Kim, A.Y.; Rhim, H.; Park, M.; Lee, M.W.; Kim, Y.S.; Choi, D.; Lim, H.K. Venous thrombosis after radiofrequency ablation for hepatocellular carcinoma. *AJR Am. J. Roentgenol.* **2011**, *197*, 1474–1480. [CrossRef]
131. Shyn, P.B.; Mauri, G.; Alencar, R.O.; Tatli, S.; Shah, S.H.; Morrison, P.R.; Catalano, P.J.; Silverman, S.G. Percutaneous imaging-guided cryoablation of liver tumors: Predicting local progression on 24-hour MRI. *AJR Am. J. Roentgenol.* **2014**, *203*, W181–W191. [CrossRef] [PubMed]
132. Shyn, P.B.; Oliva, M.R.; Shah, S.H.; Tatli, S.; Catalano, P.J.; Silverman, S.G. MRI contrast enhancement of malignant liver tumours following successful cryoablation. *Eur. Radiol.* **2012**, *22*, 398–403. [CrossRef] [PubMed]
133. Fujita, T.; Honjo, K.; Ito, K.; Arita, T.; Koike, S.; Takano, K.; Tamura, S.; Matsumoto, T.; Matsunaga, N. Fan-shaped hepatic parenchymal damage after ethanol injection therapy for hepatocellular carcinoma: MRI appearances. *Abdom. Imaging* **1999**, *24*, 56–60. [CrossRef] [PubMed]
134. Burgener, F.A.; Steinmetz, S.D. Treatment of experimental adenocarcinomas by percutaneous intratumoral injection of absolute ethanol. *Investig. Radiol.* **1987**, *22*, 472–478. [CrossRef]
135. Guan, Y.S.; Sun, L.; Zhou, X.P.; Li, X.; Zheng, X.H. Hepatocellular carcinoma treated with interventional procedures: CT and MRI follow-up. *World J. Gastroenterol.* **2004**, *10*, 3543–3548. [CrossRef]
136. Granata, V.; Fusco, R.; Catalano, O.; Piccirillo, M.; De Bellis, M.; Izzo, F.; Petrillo, A. Percutaneous ablation therapy of hepatocellular carcinoma with irreversible electroporation: MRI findings. *AJR Am. J. Roentgenol.* **2015**, *204*, 1000–1007. [CrossRef]
137. Guo, Y.; Zhang, Y.; Nijm, G.M.; Sahakian, A.V.; Yang, G.Y.; Omary, R.A.; Larson, A.C. Irreversible electroporation in the liver: Contrast-enhanced inversion-recovery MR imaging approaches to differentiate reversibly electroporated penumbra from irreversibly electroporated ablation zones. *Radiology* **2011**, *258*, 461–468. [CrossRef]
138. Paturneau-Jouas, M.; Parzy, E.; Vidal, G.; Carlier, P.G.; Wary, C.; Vilquin, J.T.; de Kerviler, E.; Schwartz, K.; Leroy-Willig, A. Electrotransfer at MR imaging: Tool for optimization of gene transfer protocols--feasibility study in mice. *Radiology* **2003**, *228*, 768–775. [CrossRef]
139. Faron, A.; Sprinkart, A.M.; Pieper, C.C.; Kuetting, D.L.R.; Fimmers, R.; Block, W.; Meyer, C.; Thomas, D.; Attenberger, U.; Luetkens, J.A. Yttrium-90 radioembolization for hepatocellular carcinoma: Outcome prediction with MRI derived fat-free muscle area. *Eur. J. Radiol.* **2020**, *125*, 108889. [CrossRef]
140. Bester, L.; Hobbins, P.G.; Wang, S.C.; Salem, R. Imaging characteristics following 90yttrium microsphere treatment for unresectable liver cancer. *J. Med. Imaging Radiat. Oncol.* **2011**, *55*, 111–118. [CrossRef]
141. Semaan, S.; Makkar, J.; Lewis, S.; Chatterji, M.; Kim, E.; Taouli, B. Imaging of Hepatocellular Carcinoma Response After (90)Y Radioembolization. *AJR Am. J. Roentgenol.* **2017**, *209*, W263–W276. [CrossRef] [PubMed]
142. Hoffmann, R.; Rempp, H.; Schraml, C.; Schwenzer, N.; Grözinger, G.; Blumenstock, G.; Rothgang, E.; Pereira, P.L.; Claussen, C.D.; Clasen, S. Diffusion-weighted imaging during MR-guided radiofrequency ablation of hepatic malignancies: Analysis of immediate pre- and post-ablative diffusion characteristics. *Acta Radiol.* **2015**, *56*, 908–916. [CrossRef] [PubMed]
143. Ibrahim, S.M.; Nikolaidis, P.; Miller, F.H.; Lewandowski, R.J.; Ryu, R.K.; Sato, K.T.; Senthilnathan, S.; Riaz, A.; Kulik, L.; Mulcahy, M.F.; et al. Radiologic findings following Y90 radioembolization for primary liver malignancies. *Abdom. Imaging* **2009**, *34*, 566–581. [CrossRef] [PubMed]
144. Shinagawa, Y.; Sakamoto, K.; Fujimitsu, R.; Ida, M.; Urakawa, H.; Kora, S.; Higashihara, H.; Takano, K.; Yoshimitsu, K. Pseudolesion of the liver observed on gadoxetate disodium-enhanced magnetic resonance imaging obtained shortly after transarterial chemoembolization for hepatocellular carcinoma. *Jpn. J. Radiol.* **2010**, *28*, 483–488. [CrossRef]

145. Koda, M.; Ueki, M.; Maeda, Y.; Mimura, K.I.; Okamoto, K.; Matsunaga, Y.; Kawakami, M.; Hosho, K.; Murawaki, Y. The influence on liver parenchymal function and complications of radiofrequency ablation or the combination with transcatheter arterial embolization for hepatocellular carcinoma. *Hepatol. Res.* **2004**, *29*, 18–23. [CrossRef] [PubMed]
146. Ebraheem Ebeed, A.; Abd El-hamied Romeih, M.; Mohamed Refat, M.; Hamdy Yossef, M. Role of dynamic contrast-enhanced and diffusion weighted MRI in evaluation of hepatocellular carcinoma after chemoembolization. *Egypt. J. Radiol. Nucl. Med.* **2017**, *48*, 807–815. [CrossRef]
147. Kloeckner, R.; Otto, G.; Biesterfeld, S.; Oberholzer, K.; Dueber, C.; Pitton, M.B. MDCT Versus MRI Assessment of Tumor Response After Transarterial Chemoembolization for the Treatment of Hepatocellular Carcinoma. *Cardiovasc. Interv. Radiol.* **2010**, *33*, 532–540. [CrossRef]
148. De Santis, M.; Alborino, S.; Tartoni, P.L.; Torricelli, P.; Casolo, A.; Romagnoli, R. Effects of lipiodol retention on MRI signal intensity from hepatocellular carcinoma and surrounding liver treated by chemoembolization. *Eur. Radiol.* **1997**, *7*, 10–16. [CrossRef]
149. Takayasu, K.; Arii, S.; Matsuo, N.; Yoshikawa, M.; Ryu, M.; Takasaki, K.; Sato, M.; Yamanaka, N.; Shimamura, Y.; Ohto, M. Comparison of CT findings with resected specimens after chemoembolization with iodized oil for hepatocellular carcinoma. *AJR Am. J. Roentgenol.* **2000**, *175*, 699–704. [CrossRef]
150. Kallini, J.R.; Miller, F.H.; Gabr, A.; Salem, R.; Lewandowski, R.J. Hepatic imaging following intra-arterial embolotherapy. *Abdom. Radiol.* **2016**, *41*, 600–616. [CrossRef]
151. Najmi Varzaneh, F.; Pandey, A.; Aliyari Ghasabeh, M.; Shao, N.; Khoshpouri, P.; Pandey, P.; Zarghampour, M.; Fouladi, D.; Liddell, R.; Anders, R.A.; et al. Prediction of post-TACE necrosis of hepatocellular carcinoma usingvolumetric enhancement on MRI and volumetric oil deposition on CT, with pathological correlation. *Eur. Radiol.* **2018**, *28*, 3032–3040. [CrossRef] [PubMed]
152. Padhani, A.R.; Liu, G.; Koh, D.M.; Chenevert, T.L.; Thoeny, H.C.; Takahara, T.; Dzik-Jurasz, A.; Ross, B.D.; Van Cauteren, M.; Collins, D.; et al. Diffusion-weighted magnetic resonance imaging as a cancer biomarker: Consensus and recommendations. *Neoplasia* **2009**, *11*, 102–125. [CrossRef]
153. Vossen, J.A.; Buijs, M.; Kamel, I.R. Assessment of tumor response on MR imaging after locoregional therapy. *Tech. Vasc. Interv. Radiol* **2006**, *9*, 125–132. [CrossRef] [PubMed]
154. Hussein, R.S.; Tantawy, W.; Abbas, Y.A. MRI assessment of hepatocellular carcinoma after locoregional therapy. *Insights Imaging* **2019**, *10*, 8. [CrossRef] [PubMed]
155. Kokabi, N.; Camacho, J.C.; Xing, M.; Edalat, F.; Mittal, P.K.; Kim, H.S. Immediate post-doxorubicin drug-eluting beads chemoembolization Mr Apparent diffusion coefficient quantification predicts response in unresectable hepatocellular carcinoma: A pilot study. *J. Magn. Reson. Imaging* **2015**, *42*, 981–989. [CrossRef]
156. Abdelhamed, W.; El-Kassas, M. Hepatocellular carcinoma recurrence: Predictors and management. *Liver Res.* **2023**, *7*, 321–332. [CrossRef]
157. Ogasawara, S.; Chiba, T.; Motoyama, T.; Kanogawa, N.; Saito, T.; Shinozaki, Y.; Suzuki, E.; Ooka, Y.; Tawada, A.; Kato, H.; et al. Prognostic Significance of Concurrent Hypovascular and Hypervascular Nodules in Patients with Hepatocellular Carcinoma. *PLoS ONE* **2016**, *11*, e0163119. [CrossRef]
158. Pecchi, A.; Besutti, G.; De Santis, M.; Del Giovane, C.; Nosseir, S.; Tarantino, G.; Di Benedetto, F.; Torricelli, P. Post-transplantation hepatocellular carcinoma recurrence: Patterns and relation between vascularity and differentiation degree. *World J. Hepatol.* **2015**, *7*, 276–284. [CrossRef]
159. Kojiro, M. 'Nodule-in-nodule' appearance in hepatocellular carcinoma: Its significance as a morphologic marker of dedifferentiation. *Intervirology* **2004**, *47*, 179–183. [CrossRef]
160. Takeda, H.; Takai, A.; Kumagai, K.; Iguchi, E.; Arasawa, S.; Eso, Y.; Shimizu, T.; Ueda, Y.; Taura, K.; Uemoto, S.; et al. Multiregional whole-genome sequencing of hepatocellular carcinoma with nodule-in-nodule appearance reveals stepwise cancer evolution. *J. Pathol.* **2020**, *252*, 398–410. [CrossRef]
161. Kang, T.W.; Rhim, H.; Song, K.D.; Lee, M.W.; Cha, D.I.; Ha, S.Y.; Ahn, J.H. Radiofrequency Ablation of Hepatocellular Carcinoma with a "Nodule-in-Nodule" Appearance: Long-Term Follow-up and Clinical Implications. *Cardiovasc. Interv. Radiol.* **2017**, *40*, 401–409. [CrossRef] [PubMed]
162. Liu, H.; Deng, H.; Hu, H.; Wu, C.; Huang, D.; Fang, C.; Yang, J.; Xiang, N. Laparoscopic Right Posterior Sectionectomy with Preservation of Subsegment Using Augmented Reality Navigation Plus ICG Fluorescence Imaging in Patients with HCC After Conversion Therapy. *Ann. Surg. Oncol.* **2024**, *31*, 5642–5644. [CrossRef] [PubMed]
163. Li, H.; Yan, W.; Zhao, J.; Ji, Y.; Qian, L.; Ding, H.; Zhao, Z.; Wang, G. Navigate biopsy with ultrasound under augmented reality device: Towards higher system performance. *Comput. Biol. Med.* **2024**, *174*, 108453. [CrossRef] [PubMed]
164. Baz, R.O.; Scheau, C.; Baz, R.A.; Niscoveanu, C. Buhler's Arc: An Unexpected Finding in a Case of Chronic Abdominal Pain. *J. Gastrointest. Liver Dis.* **2020**, *29*, 304. [CrossRef]
165. Gholizadeh, M.; Bakhshali, M.A.; Mazlooman, S.R.; Aliakbarian, M.; Gholizadeh, F.; Eslami, S.; Modrzejewski, A. Minimally invasive and invasive liver surgery based on augmented reality training: A review of the literature. *J. Robot. Surg.* **2023**, *17*, 753–763. [CrossRef]
166. Hammill, C.W.; Clements, L.W.; Stefansic, J.D.; Wolf, R.F.; Hansen, P.D.; Gerber, D.A. Evaluation of a minimally invasive image-guided surgery system for hepatic ablation procedures. *Surg. Innov.* **2014**, *21*, 419–426. [CrossRef]

167. García Vázquez, A.; Rodríguez-Luna, M.R.; Verde, J.; Piantanida, E.; Alonci, G.; Palermo, M.; Serra, E.; De Cola, L.; Giménez, M.E. Image-Guided Surgical Simulation in Minimally Invasive Liver Procedures: Development of a Liver Tumor Porcine Model Using a Multimodality Imaging Assessment. *J. Laparoendosc. Adv. Surg. Tech. Part A* **2021**, *31*, 1097–1103. [CrossRef]
168. Ravi, T.; Ranganathan, R.; Pugalendhi, A.; Arumugam, S. 3D Printed Patient Specific Models from Medical Imaging—A General Workflow. *Mater. Today Proc.* **2020**, *22*, 1237–1243. [CrossRef]
169. Timofticiuc, I.-A.; Călinescu, O.; Iftime, A.; Dragosloveanu, S.; Caruntu, A.; Scheau, A.-E.; Badarau, I.A.; Didilescu, A.C.; Caruntu, C.; Scheau, C. Biomaterials Adapted to Vat Photopolymerization in 3D Printing: Characteristics and Medical Applications. *J. Funct. Biomater.* **2024**, *15*, 7. [CrossRef]
170. Dragosloveanu, S.; Petre, M.-A.; Capitanu, B.S.; Dragosloveanu, C.D.M.; Cergan, R.; Scheau, C. Initial Learning Curve for Robot-Assisted Total Knee Arthroplasty in a Dedicated Orthopedics Center. *J. Clin. Med.* **2023**, *12*, 6950. [CrossRef]
171. Liu, R.; Abu Hilal, M.; Wakabayashi, G.; Han, H.S.; Palanivelu, C.; Boggi, U.; Hackert, T.; Kim, H.J.; Wang, X.Y.; Hu, M.G.; et al. International experts consensus guidelines on robotic liver resection in 2023. *World J. Gastroenterol.* **2023**, *29*, 4815–4830. [CrossRef]
172. Giannone, F.; Felli, E.; Cherkaoui, Z.; Mascagni, P.; Pessaux, P. Augmented Reality and Image-Guided Robotic Liver Surgery. *Cancers* **2021**, *13*, 6268. [CrossRef]